Journal of
Composites Science

MDPI

Article

Effect of Phosphogypsum Origin and Calcination Temperature on Characteristics of Supersulfated Cements

Nataliya Alfimova [1,*], Ksenia Levickaya [1,2], Ivan Nikulin [3,4], Mikhail Elistratkin [1], Natalia Kozhukhova [2,5] and Nikita Anosov [2]

[1] Building Materials Science, Products and Structures Department, Belgorod State Technological University Named After V.G. Shukhov, 46 Kostyukova Str., 308012 Belgorod, Russia; levickayalevickaya@gmail.com (K.L.); mr.elistratkin@yandex.ru (M.E.)
[2] Laboratory of Advanced Materials and Technologies, Belgorod National Research University, 85 Pobedy Str., 308015 Belgorod, Russia; kozhuhovanata@yandex.ru (N.K.); nikit.a1999@yandex.ru (N.A.)
[3] Engineering Center NRU "BelSU", 2a/712, Koroleva Str., 308015 Belgorod, Russia; ivanikulin@yandex.ru
[4] Fund of Innovative Scientific Technologies, 1, Room 3.3 Perspektivnaya Str. (Novosadovy Mkr.), Belgorod Region, Belgorod District, Novosadovy Settlement, 308518 Belgorod, Russia
[5] Department of Material Science and Material Technology, Belgorod State Technological University Named After V.G. Shukhov, 46 Kostyukova Str., 308012 Belgorod, Russia
* Correspondence: alfimovan@mail.ru; Tel.: +7-9205602511

Abstract: Supersulfated cements (SSCs) are one of the promising binders characterized by low CO_2 emissions. A significant advantage of SSC is the possibility of using phosphoanhydrite binders as a sulfate component, obtained by the calcination of phosphogypsum—a waste product of acid and fertilizer production. The utilization of phosphogypsum is a global problem. Differences in the properties of phosphogypsums from various industrial enterprises are determined by the difference in phosphate rock and the technological mode of production. This gives reason to believe that phosphoanhydrite binders (FABs) will also have differences in properties, which in turn will influence the process of structural formation of SSC. In the article, the effect of FAB produced at calcination temperatures of 600, 800, and 1000 °C using phosphogypsum of two different industrial enterprises was studied. It is established that the morphology and pH value of FAB particles, and the ratio of components in the binder have the greatest influence on the physical and mechanical characteristics of the SSC. The use of FAB with a high pH value (≈12) allows for obtaining free-of-cement SSC, with compressive strengths of up to 50 MPa at the age of 90 days.

Keywords: supersulfated cements; phosphogypsum; phosphoanhydrite binders; granulated blast furnace slag; ettringite

Academic Editor: Farshid Pahlevani

Received: 28 February 2025
Revised: 18 March 2025
Accepted: 19 March 2025
Published: 21 March 2025

Citation: Alfimova, N.; Levickaya, K.; Nikulin, I.; Elistratkin, M.; Kozhukhova, N.; Anosov, N. Effect of Phosphogypsum Origin and Calcination Temperature on Characteristics of Supersulfated Cements. *J. Compos. Sci.* **2025**, *9*, 146. https://doi.org/10.3390/jcs9040146

1. Introduction

The construction industry is one of the actively developing segments of the real sector of the economy. This causes a continuous increase in the production and consumption of various construction materials, mainly based on Portland cement (PC). The growth in demand for PCs initiates the growth of production volumes. This has a significant impact on ecology globally. On average, the specific emissions of carbon dioxide into the atmosphere per production of 1 ton of PC are 660–820 kg, depending on the properties of the raw materials and the fuel used. Taking into account the current volume of PC production, the total annual volume of CO_2 emissions reaches 3.4 million tons, which is 5–10% of the emissions of industrial areas as a whole. This leads to the growth of the "carbon footprint", which affects the global climate. In addition, cement production is

the source of a large amount of dust and is characterized by high metal consumption and multistage [1–3].

Despite the popularity of PCs due to their good properties, the above-mentioned actualizes the creation of alternative binders capable of reducing PC consumption, at least when solving basic resource-intensive construction problems. First of all, when creating alternative binders, it is extremely important to emphasize the maximum utilization of byproducts and waste, as well as to develop effective technological solutions that provide minimal environmental damage and energy consumption.

Supersulfated cement (SSC) is one of the binders that best meets the above criteria [4–6]. In most cases, the basic raw material used for the production of SSC is blast furnace granulated slag (GBFS), the content of which is 75–80% of SSC. Gypsum in the amount of 10–20% is used to activate slag solidification and to provide early strength. In some cases, an alkaline activator in the amount of about 5% is also used. As a result of the chemical reaction between the components, a cement paste consisting mainly of ettringite and C-S-H gel (CSH) is formed [5–8].

The possibility of activating GBFS with gypsum was first established in 1909 by Hans Kühl (Germany), who received the first patent for SSC [9]. In the same period of time, the main requirements that GBFS had to meet for the production of SSC were a high content of the sum of oxides CaO + MgO, and the content of aluminum oxide in the range of 14–15%. After the Second World War, due to the acute need for PC, SSC cement was widely distributed in Germany and Great Britain, and a standard was developed for SSC. However, the change in production technology for cast iron results in a decrease in the content of aluminum oxide in the slag, which is below the values required by the standard. Due to this, instead of SSC was replaced by slag cement [4].

However, nowadays, due to increased attention to the friendly use of natural resources, the number of studies aimed at developing and investigating SSC has increased significantly. This was also facilitated by the development of the new standard EN 15743:2010+A1:2015. «Supersulfated cement—composition, specifications, and conformity criteria» [10].

Initially, natural gypsum or anhydrite was used as a sulfate-bearing component for SSC production. However, a literature review shows that phosphogypsum (FG) is used as an alternative source of sulfates [11]. Interest in FG is well-founded, as it is one of the largest by-products of orthophosphoric acid and phosphate fertilizers from phosphate rocks. About 300 million tons of FG are produced annually in the world, while only 14% is utilized. The non-utilized FG is stored or dumped into reservoirs, polluting the environment [12–14]. So, the use of FG as a component of SSC increases the efficiency of its utilization.

The analysis of studies showed that for SSC production, the use of FG was considered as calcium sulfate dihydrate [15–18], sulfate semihydrate [5,15], and anhydrite [15,18,19]. The most stable results are provided when using FG in the form of anhydrite. Researchers associate this with the removal of impurities during calcination, since impurities have a negative impact on the structure formation of FG [15,19].

It should be noted that in all reviewed studies that focused on the synthesis of SSC, FG from a specific source was used. At the same time, a critical review of FGs, based on more than 65 sources presented by Bilal E. et al. [20] showed that FGs have significant differences in many parameters (chemical composition, morphology, amount of impurities, etc.). The following key factors influence the characteristics of FG: (1) the technological method of acid production, which determines the morphology of crystals; (2) the type of initial rock, which determines the amount and type of impurities.

These factors, both individually and collectively, can affect the quality of the binder based on FG. In particular, the authors of this study obtained data in [21], which showed

that FG from three different Russian enterprises differ significantly in many characteristics, which is reflected in the difference in properties (compressive and tensile strength, average density, setting time, and water consumption) of the gypsum binder. The above gives reason to believe that the initial characteristics of FG from various sources will influence the properties of phosphoanhydrite binders (FABs) and, as a result, SSC was synthesized using FABs. Such studies have not been carried out before, but they are of great practical importance, both for identifying critical factors that affect the properties of SSCs, and for rationalizing components and technological parameters of SSC production.

Thus, the subject of this manuscript was to study the effect of phosphoanhydrite binders, which were synthesized by phosphogypsum calcination at different temperatures (600, 800, and 1000 °C), using two different sources of FG, on the properties of SSC (pH value of fresh SSC, water consumption, compressive strength, and average density at the age of 2, 7, 28, and 90 days; pH value of pore space in SSC at the age of 28 days).

2. Materials and Methods

2.1. Materials

The following 2 PGs from different enterprises were used in the study:

1. FG from OOO "Phosphorit" (Kingisepp, Russia)—FG_K. Apatite concentrate of the Kovdorskoye deposit (Kovdor, Russia) of ultrabasic alkaline rocks with magmatic and metasomatic carbonatites of the Lower Paleozoic age, and organogenic phosphorites of the Karatau phosphorite-bearing basin (Zhanatas, Republic of Kazakhstan) are used as a raw material for the production of acid by this enterprise.
2. G from CJSC "FosAgro AG" (Balakovo, Russia)—FG_B. Here, the source of raw materials for acid production is the Khibina deposit of alkaline rocks of the Kola Peninsula (Apatity, Russia), with layer- and lens-shaped deposits of complex apatite ores associated with nepheline syenites.

The choice of FGs was due to the fact that phosphate rocks of various origins are the source for the production of acid at the above enterprises. In the first case (FG_K), it is a mixture of apatites and phosphorites; the second one (FG_B) is apatite. Unlike apatites, which have a volcanogenic origin, phosphorites are organic, which predetermines the presence of glauconite, limonite, calcite, dolomite, magnesium silicates, aluminosilicates, feldspars, quartz, and organic components in them [22,23]. As mentioned above, the original phosphate rock determines the amount and composition of impurities in FG. According to data in [22,23], the main impurities in apatite-based FG are residues of fluorocalcium phosphate, calcium fluoride, phosphoric acid and its compounds, silicon fluoride, silica gel, iron and aluminum sulfate, rare earth elements, sulfuric acid, and its alkaline salts. In the case of phosphorite-based FG, carbonate, sulfur compounds, aluminosilicate, and iron oxide are added to the above-mentioned components.

Visually, the PGs are bulk materials consisting of small particles and their large associations, formed through agglomeration of particles during storage under high humidity. SSA measured using the air permeability method for PG_B and PG_K was 183.9 m^2/kg; and 163.5 m^2/kg, respectively [21].

Analysis of the chemical composition of FG showed that the main oxides are CaO and SO_3. At the same time, there are differences in the content of these oxides depending on the FG source. In particular, P_2O_5 and SiO_2 are present in both samples. However, PGK contains 1.58% P_2O_5 and 1.27% of SiO_2, which is, respectively, 2.3 and 9.7 times higher than that of PGB (Table 1) [21]. Such a difference can be associated with a large number of siliceous rocks in the original phosphorite of the Karatau deposit.

Table 1. Content of oxides in the studied phosphogypsum and natural gypsum and the standard error (StdErr) of the device [21].

PG_B			PG_K		
Oxide	**%**	**StdErr%**	**Oxide**	**%**	**StdErr %**
SO_3	48.84	0.250	CaO	47.03	0.250
CaO	46.44	0.250	SO_3	46.85	0.250
SrO	2.520	0.080	P_2O_5	1.580	0.060
P_2O_5	0.684	0.034	SiO_2	1.270	0.060
CeO_2	0.362	0.018	SrO	1.050	0.050
PuO_2	0.167	0.010	F	0.980	0.170
MgO	0.145	0.008	Al_2O_3	0.319	0.016
SiO_2	0.127	0.009	CeO_2	0.216	0.011
Fe_2O_3	0.124	0.006	MgO	0.205	0.010
Na_2O	0.121	0.018	Na_2O	0.104	0.019
La_2O_3	0.119	0.009	Other	0.395	
Nd_2O_3	0.113	0.006			
Other	0.233				

XRD analysis of the studied PGs and NG demonstrated the presence of reflections responsible for the $CaSO_4 \cdot 2H_2O$ phase (d = 7.63, 4.28, 3.80, 3.07, 2.87, 2.69, 2.22, 2.08, and 1.90 Å.) (Figure 1) [21].

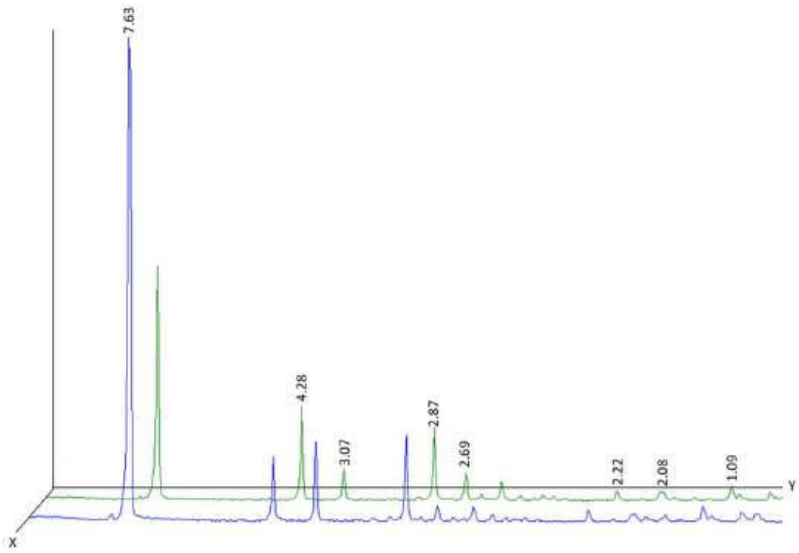

Figure 1. XRD-diagram of PGs: – PG_B; – PG_K.

More detailed analysis of FGs was previously presented by the authors in [21]. In this study, the mineral composition of FGs was additionally studied using Raman spectroscopy. Analysis of Raman spectra of PGs (Figure 2) showed that they are mostly represented by calcium sulfate dihydrate with the probable presence of a small amount of anhydrite.

It should also be noted that the peak corresponding to calcite ($CaCO_3$) was detected on spectrograms of FG_K at 278, 1086 (cm^{-1}) (Figure 2a). The presence of calcium carbonate impurities in FG_K is explained by their content in the original phosphate rock [24]. In addition, FG_K is neutralized with lime milk before storage, which can also be the reason for the presence of $CaCO_3$.

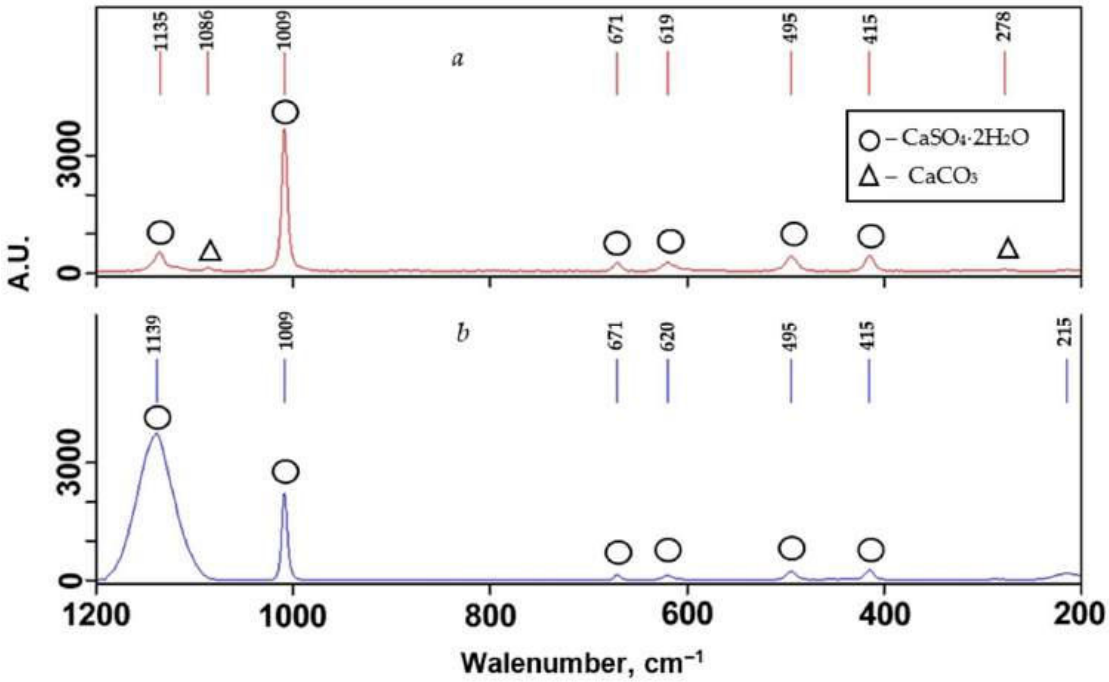

Figure 2. Raman spectra for: (**a**) FG_K; (**b**) FG_B.

Supplier of blast furnace granulated slag (GBFS) is the Public joint-stock company "Severstal" (Cherepovec, Russia). As an alkaline activator, Portland cement CEMI 42.5H from OJSC "Novoroscement" (Novorossijsk, Russia) are also used. The chemical compositions of GBFS and PC are presented in Tables 2 and 3, respectively.

Table 2. Oxides content in GBFS, wt.%.

SiO_2	CaO	Al_2O_3	MgO	TiO_2	Na_2O	SO_3	K_2O	Fe_2O_3
36.46	32.07	13.65	12.50	1.93	1.07	0.93	0.52	0.37

Table 3. Oxides content in PC, wt.%.

SiO_2	CaO	Al_2O_3	MgO	Fe_2O_3	Others
21.9	66.1	5.2	0.8	4.4	1.6

2.2. Sample Preparation and Experimental Design

Production of phosphoanhydrite binders (FABs) was carried out by calcination of FGs in a muffle furnace at 600, 800, and 1000 °C, holding them in the furnace at a given temperature for 1 h, and extracting FAB after complete cooling of the muffle furnace.

Production of SSCs was carried out by mixing GBFS, FAB, and PC in a turbulent mixer C2.0 "Vibrotehnik" (Sankt-Peterburg, Russia). GBFS and FAB were pre-milled in a laboratory ball mill to a specific surface area of 320–350 m^2/kg, which is comparable to the specific surface area of PC.

During the FAB production, it was established that an increase in the calcination temperature reduces the specific surface area of FG and increases the time required for grinding to a specific surface area (SSA) of 320–330 m^2/kg (Table 4). This phenomenon is explained by the sintering of the particles and the increase in their hardness.

To study the effect of calcination temperature, content of FAB, and PC on the properties of SSCs, a three-level matrix was designed (Table 5). The mass of GBFS in the mixture was constant, the content of FAB and PC varied according to the experiment design matrix

(Table 6). The experiment was carried out for FABs obtained using both types of FG, in parallel.

Table 4. Effect of calcination temperature and type of FG on grinding time and specific surface area (SSA) of FAB.

Parameter	Type FG and Calcination Temperature					
	FG_K			FG_B		
	600 °C	800 °C	1000 °C	600 °C	800 °C	1000 °C
SSA after calcination, m^2/kg	214.6	37.3	29.1	242.3	143.0	14.7
Grinding duration, min	1	23	49	0,5	15	47
SSA after grinding, m^2/kg	319.8	330.2	341.8	345.6	324.8	347.8

Table 5. Experiment planning conditions and parameter variation levels of the studied parameter variability interval.

Parameters		Variation Levels of Studied Parameters			Variability Interval
Original Form	Coded Form	−1	0	+1	
FAB content, % of GBFS	X_1	15	20	25	5
PC content, % of GBFS	X_2	0	3.5	7	3.5
Calcination temperature of FG, °C	X_3	600	800	1000	200

Table 6. Experiment design matrix.

No.	Input Parameters					
	Coded Form			Original Form		
	X_1	X_2	X_3	FAB * Content, % of GBFS	PC Content, % of GBFS	Calcination Temperature of FG, °C
1	+1	+1	+1	25	7	1000
2	+1	+1	−1	25	7	600
3	+1	−1	+1	25	0	1000
4	+1	−1	−1	25	0	600
5	−1	+1	+1	15	7	1000
6	−1	+1	−1	15	7	600
7	−1	−1	+1	15	0	1000
8	−1	−1	−1	15	0	600
9	+1	0	0	25	3.5	800
10	−1	0	0	15	3.5	800
11	0	+1	0	20	7	800
12	0	−1	0	20	0	800
13	0	0	+1	20	3.5	1000
14	0	0	−1	20	3.5	600
15	0	0	0	20	3.5	800

* Furthermore, the manuscript uses the abbreviations FAB_K^{600}, FAB_K^{800}, FAB_K^{1000}, FAB_B^{600}, FAB_B^{800}, and FAB_B^{1000}, where the upper index is the calcination temperature of FG when FAB production (600, 800, and 1000 °C); the lower index is the initial letter of the source FG (Kingisepp (K) or Balakovo (B)).

Samples were prepared in cubes of 2 × 2 × 2 cm (12 samples for each point of the experiment) with a W/S ratio = 0.35. A non-standard comparative method was used to study the effect of the calcination temperature and the ratio of the components in the mixture on water consumption of the SSC, which does not require a large volume of the mixture. As a characteristic of water consumption, the mini-cone flow diameter—diameter of the spread mixture on a moistened glass surface after removing the metal mini-cone (diameter of the lower base 40 mm, upper base 20 mm, and height 60 mm) and shaking

five times on a standard shaking table, used in determining the activity of PC, was used. The mini-cone flow diameter was measured in two mutually perpendicular directions, and the final value was taken as the average arithmetic value of the measurements, expressed in "mm". The obtained value reflects the water consumption of the investigated mixes, but it cannot be directly compared with the values of this parameter, measured by other methods.

Controlled output parameters are the following:

- pH value of the fresh SSC (pH);
- the mini-cone flow diameter for fresh SSC with a water content of 35% (D);
- the average density of samples dried in an oven to a constant mass at a temperature of 60 °C at the age of 2 days ($\rho_{(2)}$), 7 days ($\rho_{(7)}$), 28 days ($\rho_{(28)}$), and 90 days ($\rho_{(90)}$);
- compressive strength of samples dried to a constant mass in a drying oven at a temperature of 60 °C at the age of 2 days ($R_{(2)}$), 7 days ($R_{(7)}$), 28 days ($R_{(28)}$), 90 days ($R_{(90)}$);
- pH value of the pore space of SSC aged 28 days (pH_{28}).

2.3. Methods

An XRD analysis of the studied samples was carried out using a high-resolution diffractometer "Ultima IV" Rigaku (Rigaku, Tokio, Japan). The investigation of the mineral composition was carried out via X-ray diffraction in Cu-Kα radiation (wavelength λ = 0.154178 nm) using a Soller slit. The recording of the diffraction spectrum was carried in the range of angles 5–100 2θ; in flow mode; with scanning step Δ(2θ) = 0.02 degrees; at a speed of 2 degrees/min; operating voltage—40 kV; current flow—100 mA. The software package PDXL RIGAKU (version 2, no. 2.1.3.4) was used to refine the profile of the experimental profiles. The mineral composition was determined using the ICCD PDF-2 database (Version 2008).

The microstructure of particles of the original FG and synthesized binders, as well as the morphology of new formations in FAB and SSC was carried out by scanning electron microscopy. A scanning electron microscope Mira 3 FesSem (Tescan, Brno, Czech Republic) was used as an instrument, operating in the high vacuum mode (InBeam, Tescan, Brno, Czech Republic) using a Schottky high brightness cathode. Coating of samples was carried out with chromium (Cr).

Analysis of Raman spectroscopy was carried out on the high-sensitivity, high-resolution fiber-optic system of Raman spectroscopy i-Raman Plus (B&W Tek, Plainsboro, NJ, USA), with a laser wavelength of 785 nm.

The measurement of SSA for particles was carried out by the Bleine method on a multifunctional measuring device PSK-12 (SP) (Sankt-Peterburg, Russia).

Determination of pH value was carried out using a pH meter millivoltmeter pH 150 M (RUP "Gomelsky zavod imitritelnykh priborov", Gomel, Belarus). The solution was prepared by mixing 10 g of the solid component with 100 mL of distilled water. When determining the pH value for the pore space in the solidified SSC, before mixing with water, they were pre-filtered using a stamp.

A compressive strength test of the samples was carried out using a laboratory press with a maximum load of 10 tons.

3. Results and Discussions

3.1. Characteristics of FAB

At the first stage of study, the effect of calcination temperature on the morphology of particles and pH value of FABs was studied. It is assumed that these two parameters have a significant effect on the properties of SSC.

Morphology of FAB particles. Earlier in [20], it was established that the studied FGs belong to different morphological groups: FG_K is a mixture of the Group 1 (rhombic type)

and the Group 4 (aggregate short needle type); FG_B belongs to the Group 4 (small rhombic type). The particles of both FGs have a sufficiently developed surface (Figure 2).

Analysis of the microstructure showed that the morphology of FAB^{600} particles is similar to the morphology of the original FG particles (Figure 3). In particular, for FAB_K^{600} (Figure 4a), the presence of particles of both rhombic (Group 1) and aggregate short-needle type (Group 4) is observed. It should also be noted that, in general, FAB particles obtained at this temperature are characterized by a loose, highly developed surface.

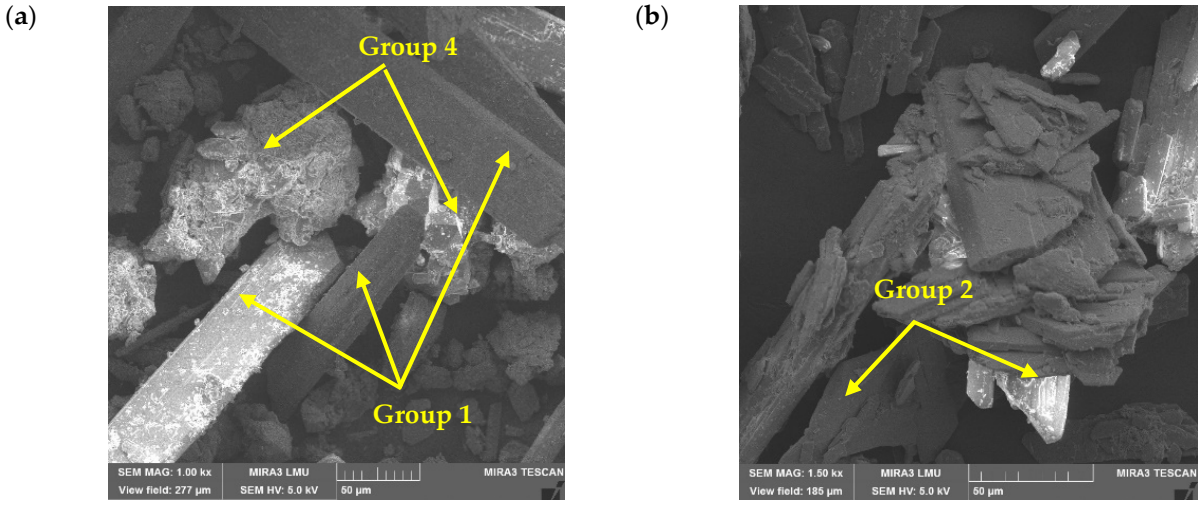

Figure 3. Morphology of FG_K (**a**), FG_B (**b**).

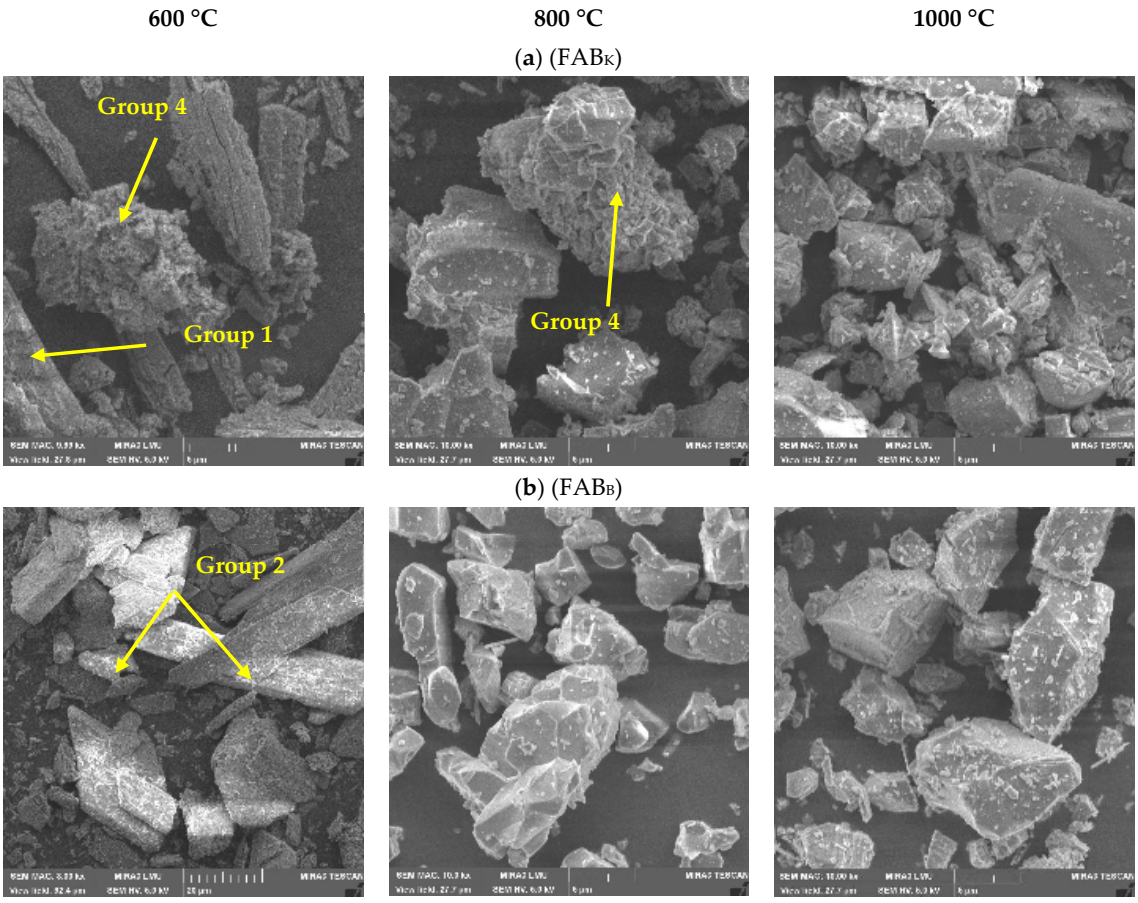

Figure 4. Morphology of FAB_K (**a**), FAB_B (**b**) after different calcination temperatures.

Under high-temperature exposure during the FAB production and during its further grinding, various processes take place that affect the shape of particles and the morphology of their surface. To reveal these changes, the FAB obtained at temperatures of 600 °C, 800 °C, and 1000 °C and ground to a specific surface of 320–330 m^2/kg was studied by electron microscopy (Figure 4).

Calcination of FAB at 800 °C and 1000 °C has a significant effect on particle morphology. At the same time, depending on the type of FG, changes occur in different ways. Most of the FAB_K^{600} particles have a compacted surface, while there are a small number of particles with the morphology of Group 4, which are characterized by a loose, highly developed surface (Figure 4a). At the same time, the morphology of the particles in FAB_K^{800}, FAB_K^{1000}, FAB_B^{800}, and FAB_B^{1000}, is similar: they do not have the characteristic features of morphological groups inherent in the particles of the original FG (Figure 4). They have an angular shape, with sharp edges and a compacted surface.

The morphology of the surface of FG particles, in this case, indicates the melting of particles and an increase in their fragility. Melting predetermines the compaction of the surface of the particles. The increase in particle fragility explains the increase in angularity during grinding.

Thus, the more developed and porous surface of FAB^{600} allows for the prediction of increased water consumption and reduced strength of SSC on its basis. The melting surface of FAB^{1000} particles has a negative effect on their grinding ability, increasing the grinding time by 2–3 times (Table 4). This leads to increased energy consumption. From this point of view, at this stage of research, the most preferred calcination temperature is 800 °C.

pH value of FG and FAB. The pH value of the medium has a great influence on hydration and structure formation in SSC [4–6], largely due to the activation of GBFS. Generally, under high-temperature exposure deformation of the crystal lattice of calcium sulfate dihydrate occurs due to which the pH value changes [25]. At the same time, the determining factors that influence the pH value of the calcium sulfate dihydrate calcination product are the origin of the gypsum-bearing raw material and the calcination temperature. In this regard, pH values were determined for FABs obtained from the studied FGs at 600 °C, 800 °C, and 1000 °C (Figure 5) and compared with pH values for FGs without temperature exposure.

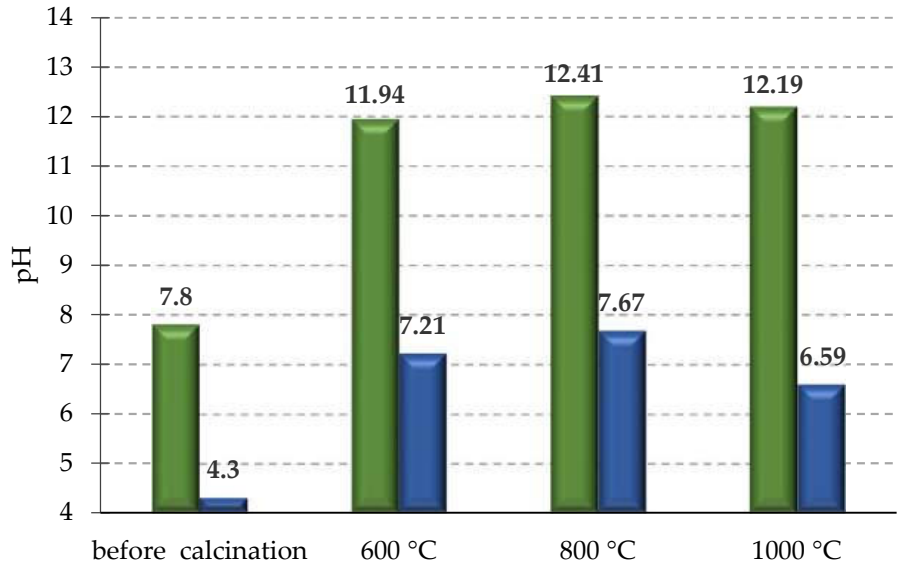

Figure 5. Dependence of pH values on calcination temperature of FG_K (■) and FG_B (■).

Analysis of the obtained results (Figure 5) showed that FABs have higher pH values compared to the original FG. Thus, calcination of FG_K in the applied temperature range leads to a shift in pH value from neutral to alkaline, and for FG_B—from acidic to neutral pH value.

Regardless of the origin of initial FG, maximum pH values are typical for FAB obtained at 800 °C; minimum pH values are typical for FAB_K obtained at 600 °C, and for FAB_B—at 1000 °C. At the same time, pH values and their increase for FAB_K are higher than pH values for FG_K. Most likely, this is due to the fact that during the FAB_K production, in addition to the removal of acid residues, decarbonization of calcite occurs with the formation of CaO, which contributes to the growth of its pH value.

It should be especially noted that the difference in pH values of FABs can have a significant impact on the structure formation when using them as a component for SSCs.

3.2. Effect of Composition and Technological Parameters on the Characteristics of SSCs

The study of the effect of composition and technological parameters on the properties of SSCs was carried out for two types of PG: FG_K (Table 7) and FG_B (Table 8).

Table 7. Controlled parameters for SSC-FG_K.

Mix ID According to (Table 6)	Average Values of Controlled Parameters and Average Statistical Deviations (%)										
	Fresh Mix		SSC-FG_K Samples								
	pH Value	Mini-Cone Flow Diameter, mm	Average Density, kg/m^3				Compressive Strength, MPa				pH_{28}
			Curing Time, Days								
			2	7	28	90	2	7	28	90	
1	11.76	98.0	1590 ± 0.1	1737 ± 1.5	1722 ± 0.9	1783 ± 1.6	6.13 ± 2.1	17.25 ± 3.9	15.50 ± 2.2	27.17 ± 4.8	11.40
2	11.58	61.9	1733 ± 0.3	1605 ± 1.4	1776 ± 1.2	1898 ± 0.6	13.21 ± 0.9	18.98 ± 3.8	16.68 ± 4.0	32.56 ± 4.2	11.36
3	11.62	94.7	1475 ± 1.0	1624 ± 0.3	1847 ± 0.6	2029 ± 0.1	2.13 ± 4.3	6.21 ± 3.4	16.23 ± 2.1	52.50 ± 4.6	11.05
4	11.24	74.4	1584 ± 0.9	1657 ± 0.8	1800 ± 0.3	2013 ± 1.5	2.00 ± 2.6	14.62 ± 4.8	21.12 ± 0.5	54.58 ± 3.7	11.05
5	11.67	96.1	1638 ± 0.5	1787 ± 1.5	1813 ± 2.3	1826 ± 2.5	8.85 ± 4.8	13.00 ± 3.7	18.88 ± 4.0	28.00 ± 1.8	11.42
6	11.54	69.0	1755 ± 0.1	1773 ± 1.1	1816 ± 1.9	1865 ± 1.9	14.75 ± 4.4	14.00 ± 3.9	29.54 ± 0.3	47.50 ± 0.1	11.37
7	11.46	90.0	1513 ± 1.2	1567 ± 1.8	1706 ± 1.6	1835 ± 1.1	1.50 ± 0.1	2.66 ± 3.1	13.85 ± 4.5	40.00 ± 0.1	11.06
8	11.08	70.9	1632 ± 0.2	1614 ± 1.8	1776 ± 4.8	1987 ± 0.6	0.53 ± 0.1	2.31 ± 3.8	18.00 ± 4.8	51.13 ± 3.9	10.85
9	11.80	80.0	1753 ± 1.5	1852 ± 1.9	1858 ± 3.5	1900 ± 4.7	9.25 ± 4.2	17.00 ± 3.3	23.58 ± 4.1	26.74 ± 2.2	11.03
10	11.64	73.9	1773 ± 0.1	1855 ± 0.7	1786 ± 3.2	1902 ± 0.6	7.13 ± 1.7	14.25 ± 3.5	18.18 ± 0.2	31.71 ± 4.1	11.05
11	11.75	79.7	1806 ± 2.7	1869 ± 3.2	1812 ± 0.9	1871 ± 0.4	14.29 ± 0.1	13.00 ± 4.4	23.17 ± 1.9	38.88 ± 4.7	11.22
12	11.65	86.4	1589 ± 1.0	1701 ± 1.6	1797 ± 0.8	1983 ± 0.2	2.56 ± 4.5	9.79 ± 3.8	22.48 ± 0.9	50.00 ± 0.1	10.90
13	11.67	95.8	1609 ± 2.4	1640 ± 0.7	1651 ± 1.1	1763 ± 1.2	7.50 ± 4.6	8.00 ± 3.4	10.83 ± 3.9	24.13 ± 2.7	11.00
14	11.52	70.0	1726 ± 1.4	1720 ± 3.3	1676 ± 0.5	1908 ± 1.1	9.02 ± 2.4	14.36 ± 4.5	13.00 ± 1.3	33.02 ± 4.0	10.89
15	11.77	86.4	1721 ± 1.1	1791 ± 1.9	1778 ± 0.7	1766 ± 0.7	7.05 ± 3.2	11.66 ± 3.3	14.42 ± 4.1	25.00 ± 0.1	11.11

Table 8. Controlled parameters for SSC-FG_B.

Mix ID According to (Table 6)	Average Values of Controlled Parameters and Average Statistical Deviations (%)										
	Fresh Mix		SSC-FG_B Samples								
	pH Value	Mini-Cone Flow Diameter, mm	Average Density, kg/m^3				Compressive Strength, MPa *				pH_{28}
			Curing Time, Days								
			2	7	28	90	2	7	28	90	
1	11.57	94.5	1634 ± 0.3	1800 ± 0.8	1737 ± 3.4	1847 ± 0.6	9.90 ± 4.7	12.13 ± 3.1	17.15 ± 3.3	29.50 ± 4.8	11.16
2	11.57	59.8	1608 ± 0.5	1746 ± 1.7	1755 ± 0.1	1803 ± 0.2	9.50 ± 4.5	11.25 ± 2.9	16.88 ± 0.7	31.75 ± 2.7	11.15
3	10.47	100.9	1519 ± 0.4	1712 ± 0.3	1770 ± 0.8	1910 ± 2.9	–	–	3.66 ± 3.9	19.11 ± 4.7	9.71
4	10.63	56.1	1545 ± 0.3	1632 ± 3.2	1713 ± 1.0	1839 ± 4.9	–	–	4.58 ± 4.1	21.01 ± 3.5	10.12
5	11.58	95.8	1588 ± 1.7	1738 ± 1.0	1793 ± 1.2	1823 ± 1.9	8.00 ± 4.8	17.13 ± 2.8	27.00 ± 3.8	32.96 ± 3.3	11.22
6	11.54	72.20	1645 ± 1.8	1726 ± 2.9	1767 ± 1.7	1811 ± 0.2	10.76 ± 0.1	14.73 ± 4.5	31.25 ± 3.7	39.25 ± 2.8	11.22
7	10.70	105.20	1654 ± 3.2	1629 ± 0.2	1684 ± 1.1	1864 ± 1.1	–	–	4.25 ± 2.8	24.25 ± 2.2	9.73
8	10.61	93.90	1611 ± 0.4	1634 ± 2.7	1669 ± 1.2	1863 ± 2.1	–	–	7.54 ± 4.3	36.58 ± 3.1	10.22
9	11.50	92.80	1620 ± 0.4	1734 ± 1.0	1729 ± 2.2	1855 ± 1.8	5.00 ± 4.1	8.01 ± 4.1	16.28 ± 2.3	20.91 ± 3.6	11,15
10	11.49	92.00	1668 ± 0.9	1756 ± 1.9	1693 ± 2.6	1840 ± 0.3	4.39 ± 2.4	10.11 ± 3.9	11.31 ± 3.5	18.41 ± 4.1	11.16
11	11.55	96.80	1658 ± 0.1	1870 ± 0.3	1836 ± 0.7	1796 ± 0.3	6.6 ± 0.1	14.50 ± 3.2	21.91 ± 4.1	30.00 ± 2.5	11.11
12	10.69	100.30	1681 ± 2.1	1617 ± 1.8	1732 ± 3.0	1780 ± 1.3	–	–	6.16 ± 3.8	18.41 ± 1.0	10.42
13	11.50	96.80	1584 ± 1.8	1695 ± 2.3	1689 ± 0.4	1811 ± 0.9	6.75 ± 0.1	8.81 ± 0.1	12.67 ± 4.2	16.96 ± 4.2	11.12
14	11.51	66.10	1618 ± 0.5	1689 ± 1.2	1720 ± 1.4	1788 ± 0.7	7.37 ± 0.1	8.13 ± 3.2	16.67 ± 3.7	26.05 ± 3.4	11.00
15	11.43	95.30	1684 ± 0.7	1691 ± 0.6	1694 ± 1.1	1810 ± 3.3	4.29 ± 3.7	6.38 ± 3.9	14,04 ± 3.4	24.43 ± 3.2	11.06

* The absence of a value indicates that the compressive strength of the mix at this age was too low to be determined using a press.

3.2.1. Effect of Composition and Technological Parameters on Mini-Cone Flow Diameter of Fresh SSCs

After statistical computer processing of the experimental data, the followings regression Equations (1) and (2) were obtained that allows to describe the effect of variable factors on the cone flow diameter of fresh SSCs:

$$D_K = 82.21 + 0.91X_1 - 1.17X_2 + 12.84X_3 - 4.22X_1^2 + 1.88X_2^2 + 1.73X_3^2 - 1.68X_1X_2 + 1.28X_1X_3 + 2.98X_2X_3 \quad (1)$$

$$D_B = 94.23 - 5.50X_1 - 3.73X_2 + 14.51X_3 - 1.57X_1^2 + 4.58X_2^2 - 12.52X_3^2 + 3.55X_1X_2 + +5.58X_1X_3 + 0.28X_2X_3 \quad (2)$$

Analysis of the obtained regression equations showed that at "0" values of all factors (FAB content = 20%; PC content = 3.5%; Calcination temperature of FG = 800 °C), Mini-cone flow diameter for SSC_B is 12 mm larger than for SSC_K. This difference is explained by the fact that in FAB_K^{800} there are particles with a fairly developed surface (Figure 4a) and, most likely, porosity, which contributes to the increase in the water consumption.

Also, the analysis of the regression Equations (1) and (2) demonstrated that in both cases, the most significant factor influencing the mini-cone flow diameter is the calcination temperature of FG (X_3): the higher the calcination temperature, the greater the mini-cone flow diameter. This can be explained by the significant influence of calcination temperature on particle surface morphology (Figure 4). FAB particles obtained at 600 °C have a loose and highly developed surface, while the surface of FAB particles obtained at 800 °C and 1000 °C is compact.

Analysis of nomograms (Figure 6), plotted on the basis of regression Equations (1) and (2), showed that in the case of using FAB_K (Figure 6a) at all studied calcination temperatures of FG_K, graphs have a similar profile with minor differences.

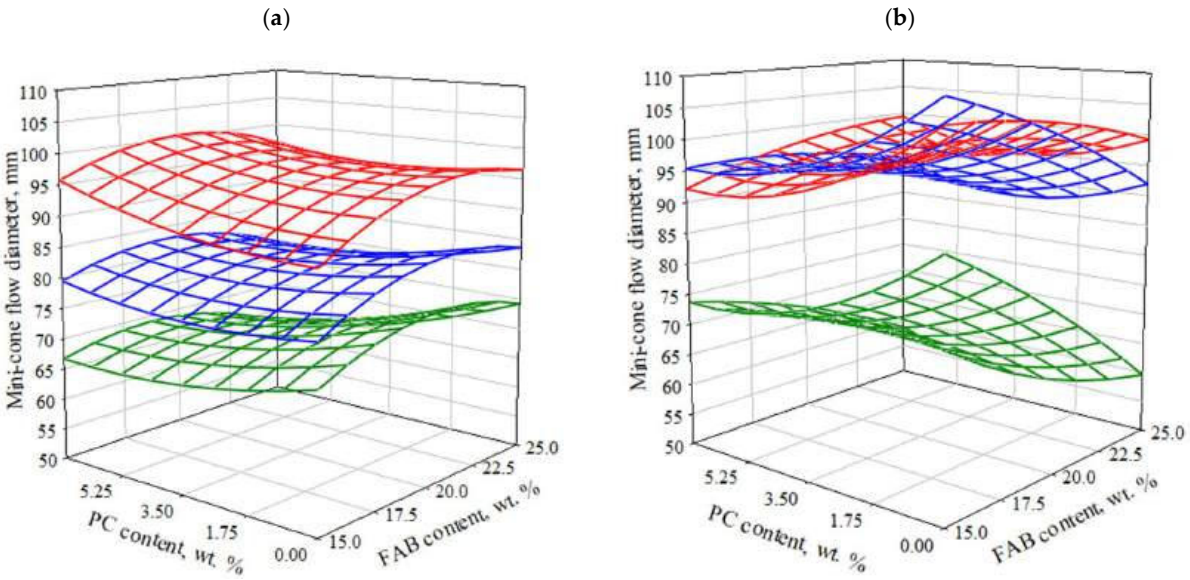

Figure 6. The effect of the content of FAB_K (**a**), FAB_B (**b**), and PC on the mini-cone flow diameter of SSC depending on the calcination temperature of FG: ■—600 °C; ■—800 °C; ■—1000 °C.

In particular, regardless of the calcination temperature of FG_K and free-of-cement SSC_K, the mini-cone flow diameter increases with an increase in the content of FAB_K in the mixture. It should also be noted that when using FAB_K^{600}, an increase in PC content in SSC_K leads to a decrease in the mini-cone flow diameter (Figure 6a), regardless of its content in the mixture. When using FAB_K^{1000}, an inverse relationship is observed: with an increase, the PC content, mini-cone flow diameter increases (Figure 6a). At the same time, when

using FAB_K^{800} an increase in the proportion of PC in SSC_K, there is practically no effect on the mini-cone flow diameter (Figure 6a).

The analysis of the dependence of the water consumption of SSC on various factors allowed to reveal (Figure 6b) that at any calcination temperature, at 15% content of FAB in SSC, an increase in the proportion of PC in the mixture leads to a decrease in the mini-cone flow diameter, and at a content of 25% of FAB_B^{600} an increase in the proportion of PC in the mixture is not reflected in the mini-cone flow diameter (Figure 6b). At the same time, when using FAB_B^{800} and FAB_B^{1000} (Figure 6b), an increase in the content of PC up to ≈3.5% contributes to a decrease, and a further increase in PC leads to an increase in the mini-cone flow diameter.

The maximum mini-cone flow diameter is observed for free-of-cement SSC_B with a minimum content of FAB_B (15% of the mass of GBFS) regardless of the calcination temperature (Figure 6b).

It is also necessary to note that with the increase in the calcination temperature of FG, a uniform and approximately equal increase in the mini-cone flow diameter, which is 13 mm, is observed at each interval of 200 °C. At the same time, the mini-cone flow diameter for SSC_B, produced using FAB_B^{800} and FAB_B^{800}, lies in narrow ranges and, on average, is 98.5 and 99 mm, respectively. The average mini-cone flow diameter for binders based on FAB_B^{600} is 71 mm.

Thus, it turns out that for SSC_K^{600} (Figure 6a) and SSC_B^{600} (Figure 6b), as well as for SSC_K^{1000} (Figure 6a) and $SSC_Б^{1000}$ (Figure 6b), the mini-cone flow diameters are in approximately equal ranges. At the same time, the mini-cone flow diameter for SSC_B^{800}, as already noted earlier, is on average 12 mm larger than the mini-cone flow diameter for SSC_B^{800}. This indicates that the initial characteristics of FG and calcination temperature affect the surface morphology of FAB particles, which is reflected in the morphology of particles and water consumption of SSC and, as a result, is reflected in the physical and mechanical characteristics of the final products.

3.2.2. Effect of Composition and Technological Parameters on the pH Value of Water Extract Based on SSC

After statistical computer processing of experimental data, the following regression equations were obtained, which allows for describing the influence of variable factors on pH value of extract based on SSC:

$$pH_K = 11.76 + 0.06X_1 + 0.13X_2 + 0.12X_3 - 0.04X_1^2 - 0.06X_2^2 - 0.17X_3^2 - 0.02X_1X_2 - 0.06X_2X_3 \quad (3)$$

$$pH_B = 11.49 - 0.02X_1 + 0.47X_2 - 0.01X_1^2 - 0.39X_2^2 + 0.03X_1X_2 - 0.04X_1X_3 + 0.01X_2X_3 \quad (4)$$

The analysis of the regression Equations (3) and (4) showed that the content of PC in the mixture (X_2) is the most significant variable factor of the three ones, affecting the growth of pH values, regardless of the type of FAB. This is due to the fact that among all the components of the mix, PC has the highest pH value and is capable of active hydrolysis with the release of $Ca(OH)_2$. When using FAB_B, which is characterized by lower pH values (see Figure 4), changing the content of PC will have a greater effect on pH value than when using FAB_K. This is indicated by the coefficient of $0.47X_2$ (Equation (3)). At the same time, the increase in the proportion of FAB_K (factor X_1) contributes to the increase in pH values, while when using FAB_B, a weaker but inverse relationship is naturally observed. When using FAB_B, the calcination temperature for FG (factor X_3) practically does not affect the pH value (the coefficient before factor X_3 is equal to 0.003), so this factor was excluded from the regression Equation (4).

Based on the obtained regression equations, graphical dependences (nomograms) of pH value on variable factors were plotted (Figure 7). Character nomograms showed that when using FAB_K, its pH values change or vary significantly in the range of 11.08–11.80.

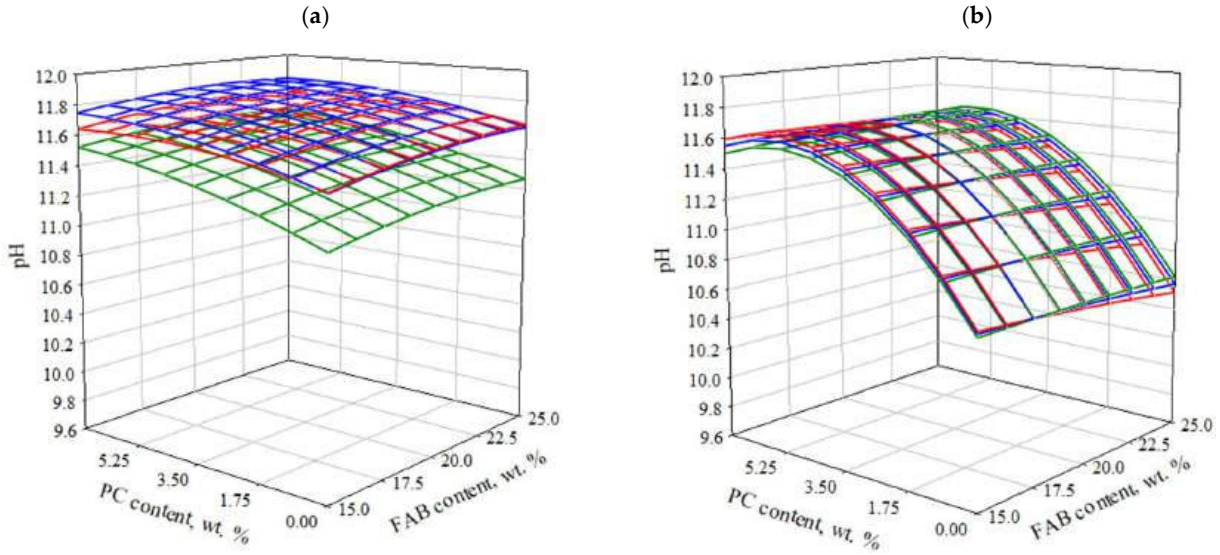

Figure 7. The influence of the content of FAB_K (**a**), FAB_B (**b**), and PC on the pH value of the aqueous extract from SSCs at different calcination temperatures of FGs: ■—600 °C; ■—800 °C; ■—1000 °C.

For FAB_B, this range is 10.61–11.57. When using FAB_K, at the studied calcination temperatures, minimum pH values are observed in SSC_K with 15% content of FAB_K ($X_1 = -1$) without PC ($X_2 = -1$); maximum pH values are observed at 25% content of FAB_K ($X_1 = +1$) and 7% of PC ($X_2 = +1$) (Figure 7a).

At the same time, an increase in the calcination temperature of FG in the production of FAB_K contributes to the increase in the alkalinity of SSC_K (Figure 7a). Regardless of the content of FAB and PC, the lowest pH values are characteristic of SSC_K produced with FAB_K^{600} (Figure 7a); the highest pH values are characteristic of SSC_K produced using FAB_K^{800} and with a content of 7% PC (by wt. of GBFS) (Figure 7b). With a lower content of PC or its absence, pH values of SSC_K, based on FAB_K, calcined at 800 °C and 1000 °C are comparable (Figure 7a).

The nature of the dependence of pH values on variable factors when using FAB_B differs from the dependence for FAB_K. Thus, in the absence of PC and with an increase in FAB_B, a decrease in pH values is observed. Moreover, the higher the calcination temperature, the more noticeable this tendency (Figure 7b). The minimum pH value = 10.51 is typical for SSC_B containing PC with 25% content of FAB_B^{1000} (Figure 7b). This is quite natural and is explained by lower pH values (6.59) for FAB_B^{1000}, compared to FAB, obtained at calcination temperatures of 600 and 800 °C (Figure 4).

Also, as in the case of FAB_K, regardless of its content and calcination temperature, an increase in the content of PC in SSCB contributes to an increase in pH value (Figure 7b). However, it should be noted that in the case of FAB_B, a more significant increase in pH value is observed when the PC content increases from 0 to 5.25% (approximately 11.5%).

Based on the revealed dependencies and significant differences in the profiles of the nomograms, which show the dependence of the pH value on various factors, it is possible to conclude that the features of the initial FG, determined by the origin of the phosphate rock, have a significant impact on the pH value of FABs and, as a result, on the pH value of SSC. At this stage of research, it is possible to assume that the most likely SSC produced with FAB_K will be strengthened even in the absence of an alkaline component (PC), since the pH value for SSC_K, even without PC, is within the required limits that ensure the

activation of GBFS and the processes of structure formation. On the other hand, when using FAB_B, the absence of PC in SSC is critical. pH values of free-of-cement SSC_B (Mixes 3, 4, 7, 8, 12, Table 8) are located outside the lower limit: 10.8–12.5 [6,14], required for the flow of structural formation processes in SSC. Probably, free–of-cement SSC_B will have low or even "0" compressive strength in the early period of hardening.

3.2.3. The Effect of Composition and Technological Parameters on the Average Density of Consolidated SSC

Comparative analysis of regression Equations (5)–(12) obtained by processing experimental values of average density of SSC at the age of 2, 7, 28 and 90 days (Equations (5)–(12)) was performed to reveal regularities describing the effect of variable factors on the average density and predicting their possible changes over time.

$$\rho_{K(2)} = 1746.24 - 17.60X_1 + 72.90X_2 - 60.50X_3 + 10.44X_1^2 - 55.06X_2^2 - 85.06X_3^2 + 2.00X_1X_2 - 2.00X_1X_3 - 4.00X_2X_3 \quad (5)$$

$$\rho_{K(7)} = 1817.26 - 18.38X_1 + 54.52X_2 - 7.68X_3 + 29.68X_1^2 - 38.82X_2^2 - 47.60X_1X_2 + 8.65X_1X_3 + 20.40X_2X_3 \quad (6)$$

$$\rho_{K(28)} = 1760.94 + 10.44X_1 + 1.29X_2 - 10.43X_3 + 65.39X_1^2 + 48.04X_2^2 - 93.23X_3^2 - 37.04X_1X_2 + 8.35X_1X_3 - 4.25X_2X_3 \quad (7)$$

$$\rho_{K(90)} = 1846.90 + 20.93X_1 - 60.47X_2 - 43.64X_3 + 34.14X_1^2 + 59.82X_2^2 - 31.40X_3^2 - 28.81X_1X_2 + 11.47X_1X_3 - 2.23X_2X_3 \quad (8)$$

$$\rho_{B(2)} = 1664.84 - 24.18X_1 + 12.35X_2 - 4.77X_3 - 16.40X_1^2 + 9.40X_2^2 - 58.67X_3^2 + 26.13X_1X_2 + 1.75X_1X_3 - 6.05X_2X_3 \quad (9)$$

$$\rho_{B(7)} = 1725.27 + 14.10X_1 + 65.60X_2 + 14.70X_3 + 11.17X_1^2 + 9.67X_2^2 - 41.83X_3^2 + 0.13X_1X_2 + 15.88X_1X_3 - 1.13X_2X_3 \quad (10)$$

$$\rho_{B(28)} = 1721.25 + 9.74X_1 + 31.96X_2 + 9.94X_3 - 16.91X_1^2 + 56.36X_2^2 - 23.17X_3^2 - 24.68X_1X_2 - 0.31X_1X_3 - 8.15X_2X_3 \quad (11)$$

$$\rho_{B(90)} = 1799.33 + 5.30X_1 - 17.60X_2 + 15.10X_3 + 50.83X_1^2 - 8.67X_2^2 + 2.83X_3^2 - 0.75X_1X_2 + 12.75X_1X_3 - 2.00X_2X_3 \quad (12)$$

Analysis of the regression equations allowed us to reveal a number of the following regularities. Regardless of the type of FG, at "zero" values of all variable factors (FAB content = 20%; PC content = 3.5%; calcination temperature of FG = 800 °C), a decrease in the average density of SSC at the age of 28 days compared to 7 days is observed, with a subsequent increase in the average density at the age of 90 days. This can indicate the realization of recrystallization processes. The greatest changes in the average density in the studied interval of hardening time are observed in SSC_K. It should also be noted that the average density of SSC_K in "zero" values at the age of 2 and 7 days is approximately 5% higher, and at the age of 28 and 90 days is approximately 2.5% higher than the average density of similar mixes of SSC_B.

Among the general regularities for both types of SSC, a positive effect of increasing PC content in the average density of samples at the age of 2, 7, and 28 days and a negative effect at the age of 90 days is observed.

It is noted that the value, the importance of variable factors, and the nature of their influence (positive or negative) on the average density, and, therefore, on the process of structure formation, changes not only over time but also depending on the type of FG used.

Using the obtained regression Equations (5)–(12), nomograms of dependence of the average density of SSC on variable factors and time of hardening were plotted (Figure 8).

The analysis of the plotted nomogram showed that the type of FAB determines the nature of the influence of variable factors on the average density, which is expressed in the difference between the nomogram profiles (Figure 8a,b). At the same time, for each SSC, when the calcination temperature changes, the nomogram profile has a similar character, but the profile changes significantly depending on the hardening time.

It should also be noted that regardless of the type of FAB, with an increase in the hardening time, an increase in the average density of SSC is observed (Figure 8). This can indicate the chemical binding of water in the mixture to the formation of ettringite and other hydrated phases.

The analysis of the effect of FAB production temperature on the average density showed that SSC produced using FAB obtained at 800 °C has the highest average density; and at 1000 °C—the lowest average density, regardless of the hardening time. At the same time, the average density for SSC_K^{600} has an intermediate value: at the age of 7 and 28 days, their values are close to the values for SSC_K^{1000}. At the age of 90 days, these values are similar, and with a certain proportion of PC in the mix, the average density slightly exceeds the values for SSC_K^{800} (Figure 8a).

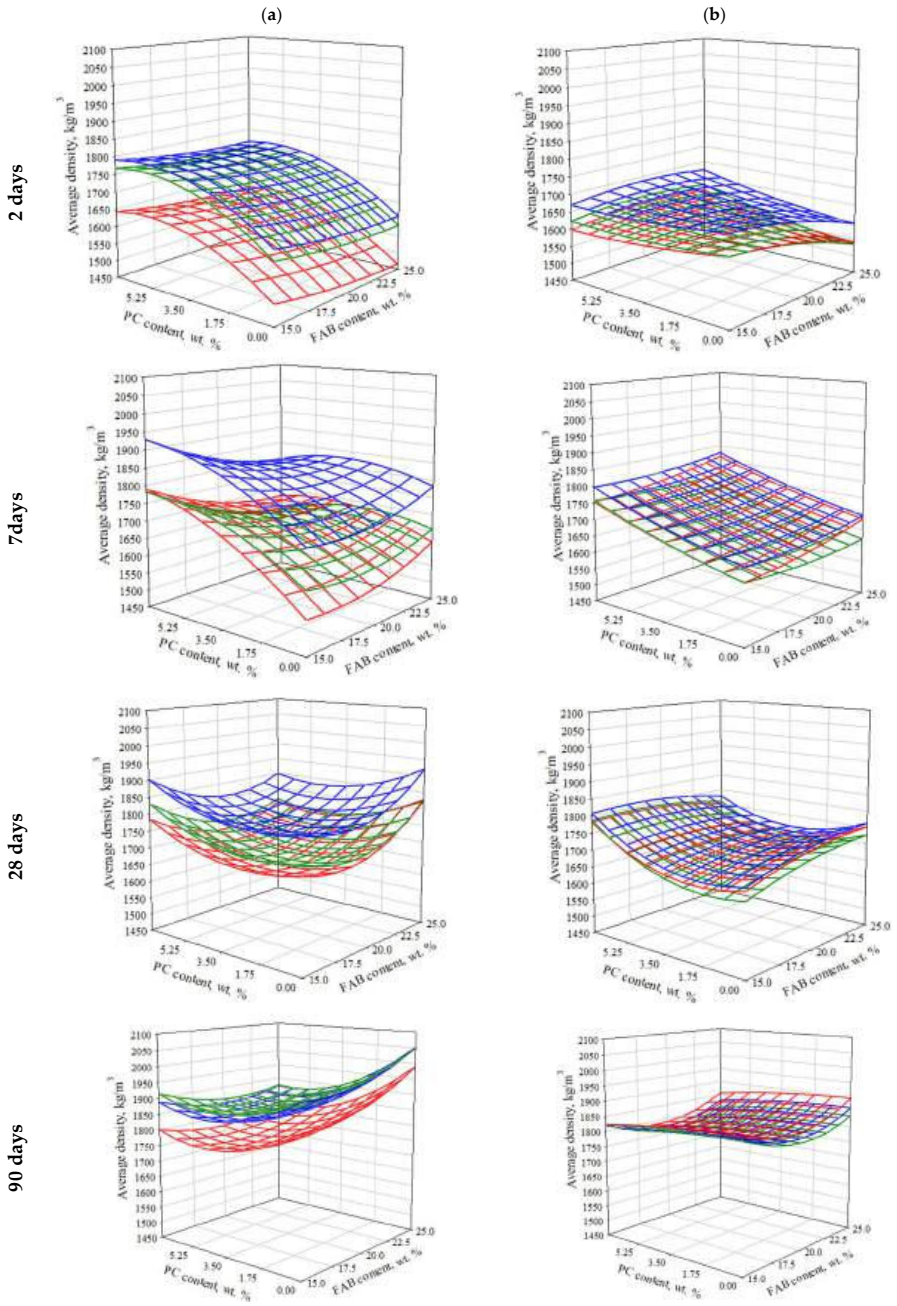

Figure 8. Effect of content of FAB_K (**a**), FAB_B (**b**), and PC (wt.% of GBFS) on the average density of consolidated SSCs at the age of 2, 7, 28, and 90 days at different production temperatures of FAB: ■—600 °C; ■—800 °C; ■—1000 °C.

SSC_B, produced with the use of FAB_B^{800}, and at 90 days—with the use of FAB_B^{1000} are characterized by the highest average density at the age of 2, 7, 28 days. Distances between graphic surfaces for SSC_B (Figure 8b) are significantly smaller than for SSC_K (Figure 8a). This indicates that for FAB_K, the temperature of its production has a stronger influence

on the change in the average density of SSC, which is confirmed by higher values of the coefficient for X_3 in regression Equations (5)–(8).

The obtained results give reason to believe that, in the absence of PC in SSC and when using a less alkaline sulfate component, structure formation and hardening proceed much more slowly, as evidenced by the lower values of the average density at the age of 2 and 7 days, and in the case of SSC_B at 28 days, as well. In addition, these factors can determine the predominant composition of the formed hydrate phases, the influence of which on the average density is determined by different amounts of bound water.

3.2.4. Effect of Composition and Technological Parameters on Compressive Strength of SSCs

To reveal the influence of variable factors and time on compressive strength of SSCs, a comparative analysis of regression equations obtained from the processing of experimental values of compressive strength at the age of 2, 7, 28 and 90 days was performed (Equations (13)–(20)).

$$R_{K(2)} = 8.68 - 0.03X_1 + 4.83X_2 - 1.37X_3 - 0.91X_1^2 - 0.67X_2^2 - 0.84X_3^2 - 0.76X_1X_2 - 0.22X_1X_3 - 1.73X_2X_3 \quad (13)$$

$$R_{K(7)} = 13.60 + 2.08X_1 + 5.31X_2 - 0.69X_3 + 1.04X_1^2 + 0.53X_2^2 - 4.49X_3^2 - 0.26X_1X_2 - 0.62X_1X_3 + 0.10X_2X_3 \quad (14)$$

$$R_{K(28)} = 17.28 - 0.53X_1 + 1.21X_2 - 2.31X_3 + 2.88X_1^2 + 4.83X_2^2 - 6.09X_3^2 - 2.72X_1X_2 + 1.09X_1X_3 - 0.35X_2X_3 \quad (15)$$

$$R_{K(90)} = 28.75 - 0.47X_1 - 7.4X_2 - 4.70X_3 - 0.47X_1^2 + 14.74X_2^2 - 1.12X_3^2 - 3.97X_1X_2 + 2.89X_1X_3 - 1.46X_2X_3 \quad (16)$$

$$R_{B(2)} = 4.91 + 0.12X_1 + 4.48X_2 - 0.30X_3 - 0.37X_1^2 - 1.73X_2^2 + 2.00X_3^2 + 0.08X_1X_2 + 0.39X_1X_3 - 0.30X_2X_3 \quad (17)$$

$$R_{B(7)} = 8.20 - 1.06X_1 + 6.97X_2 + 0.40X_3 + 0.41X_1^2 - 1.40X_2^2 - 0.18X_3^2 - 1.06X_1X_2 - 0.19X_1X_3 + 0.41X_2X_3 \quad (18)$$

$$R_{B(28)} = 14.18 - 2.28X_1 + 8.80X_2 - 1.22X_3 - 0.41X_1^2 - 0.17X_2^2 + 0.46X_3^2 - 2.59X_1X_2 + 0.86X_1X_3 + 0.03X_2X_3 \quad (19)$$

$$R_{B(90)} = 19.88 - 2.92X_1 + 4.41X_2 - 3.19X_3 + 0.92X_1^2 + 5.46X_2^2 + 2.76X_3^2 + 1.22X_1X_2 + 1.81X_1X_3 + 0.71X_2X_3 \quad (20)$$

The analysis of regression equations allowed for the following regularities to be revealed. At "zero" values of all factors, with an increase in the hardening time, a continuous increase in compressive strength is observed. At the same time, SSC_K is the leader within the studied time interval.

An increase in PC content in SSC (factor X_2) has a positive effect on compressive strength up to 28 days. At the same time, for SSC_B, the PC content is the most significant factor during the studied hardening period (Equations (17)–(20)). In the case of SSC_K, the positive effect of the amount of PC (factor X_2) on strength decreases in the period from 2 to 28 days, and at the age of 90 days, it acquires a negative value: the higher the PC content, the lower the compressive strength of SSC.

The temperature of FAB production (factor X_3) has the greatest influence on the change in compressive strength for SSC_K. This is evidenced by the high values of the coefficient X_3 in Equations (13)–(16) compared to the values of the coefficient X_3 in Equations (17)–(20).

Based on the equations obtained, graphic dependence of the compressive strength of SSCs on various factors and the time of hardening were plotted (Figure 9).

The analysis of the plotted nomogram allowed us to establish that regardless of the type of FAB, the compressive strength of all SSCs increases with an increase in the hardening time (Figure 9). Also, for each SSC, the profile of the nomogram has a similar character when the calcination temperature changes. However, for SSC_K nomograms, the distance between the graphic surfaces is greater, which, as already noted earlier, indicates a stronger influence of the FAB production temperature on compressive strength. The specified regularities are correlated with the regularities of the effect of variable factors on the average density (Figure 8).

Comparison of nomograms for SSC_K and SSC_B showed that at the age of 2 and 7 days, the profiles are very similar and represent a surface without significant bends. At the same time, the maximum compressive strength (independent of FAB content and production temperature) is typical for SSC with the maximum PC content (7%), and the minimum strength is in SSC without PC. For SSC_B at the age of 28 days, these dependencies are preserved; character surface nomogram is preserved.

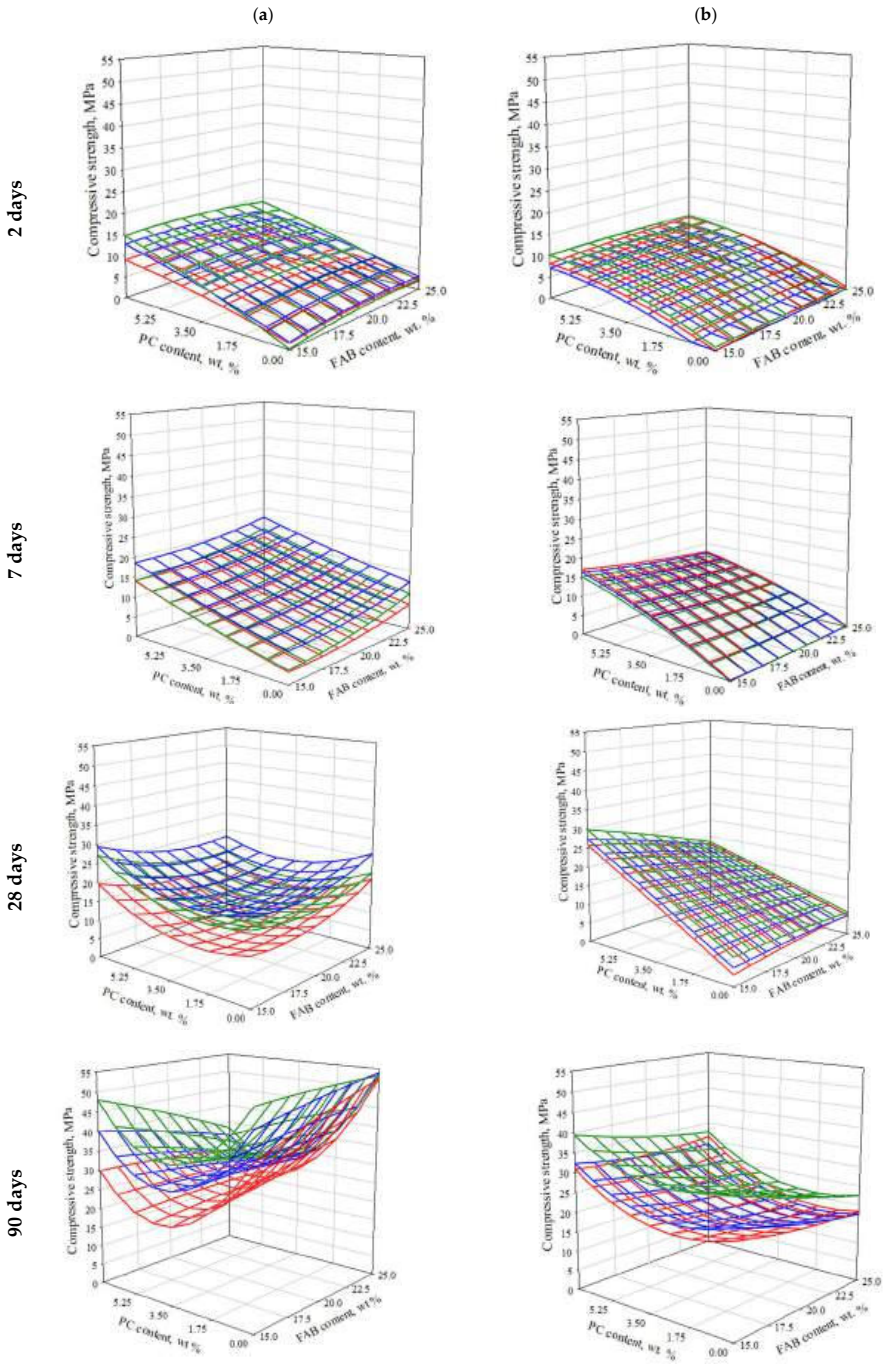

Figure 9. Effect of the content of FAB_K (**a**), FAB_B (**b**), and PC (% of GBFS) on the compressive strength of SSC at the age of 2, 7, 28, and 90 days at different production temperatures of FAB ■—600 °C; ■—800 °C; ■—1000 °C.

For SSC_K, due to the significant increase in compressive strength without PC, their values are comparable, and in some cases, they exceed the values for SSC_K with a maximum

content of PC. As the hardening time increases, the deflection of the nomogram in the central area is formed and becomes more noticeable.

For SSC_B, the deflection in the central area of the nomogram appears only at the age of 90 days. At the same time, the compressive strength of free-of-cement SSC_B is on average 10 MPa lower than for SSC_B with the maximum PC content.

The calcination temperature of FG has different effects on increases in the strength of SSC_K and SSC_B, with an increase in hardening time. For SSC_K, at the age of 2 and 90 days, SSC containing FAB_K^{600} demonstrate the highest strength, and at the age of 7 and 28 days—FAB_K^{800}. At the same time, SSC_K^{1000} is characterized by the lowest strength in the studied time interval.

Most likely, this is due to the increase in the calcination temperature, FG particles are compacted, which can cause a decrease in the reactivity of SSC and, as a result, a decrease in its strength.

Particles of FAB_K^{600} are distinguished by a more developed surface and porosity (Figure 4), and as a result, greater water permeability and reactivity. This ensures more intense formation of ettringite and increased strength in the initial period of hardening (2 days) (Figure 9). At the same time, excessively intensive formation of ettringite can contribute to the blocking of the surface of GBFS particles and thereby slow down the process of structure formation of SSC_K^{600}. Probably, from this point of view, FAB_K^{800} occupies an intermediate position in reactivity, and therefore, at the age of 7 and 28 days, SSC_K^{800} differs in greater compressive strength values. In the later period, most likely, recrystallization of new formations blocking GBFS occurs, hardening is activated again, and by 90 days, the strength of SSC_K^{600} again begins to exceed the strength of SSC_K^{800}.

In the case of SSC_B, the strength of $SSC_Б^{600}$ exceeds the strength of $SSC_Б^{800}$ and $SSC_Б^{1000}$ during almost the studied period of hardening (except for 7 days). Since the strength and average density of SSC_B is lower than for SSC_K, it can be assumed that FAB_B, due to lower pH values compared to FAB_K, provides the growth of a smaller number of new formations per unit time, due to which the surface of GBFS particles remains accessible to water for a longer time and ion exchange with a porous medium. For SSC_B, the process of structure formation occurs more smoothly, in the entire volume, and not only near the surface of GBFS particles. The main factor affecting the strength of SSC_B is the activity of FAB, which, as already noted earlier, naturally decreases with increasing calcination temperature of FG.

However, despite the fact that the use of FAB^{600} makes it possible to produce SSC with the highest compressive strength at the age of 90 days, the morphology of the surface of FAB particles (Figure 4) contributes to the fact that SSC^{600}, in comparison with SSC^{800} and SSC^{1000}, has a significantly greater water consumption (Tables 7 and 8). In the case of preparing mixes with equal flowability, SSC^{600} will have lower compressive strength compared to SSC^{800}.

An additional experiment was carried out to confirm this hypothesis. These formed samples SSC_K^{600}, SSC_K^{800}, and SSC_K^{1000} are 2 × 2 × 2 cm in size, with similar content of FAB (15% of GBFS) and PC (7% of GBFS). At the same time, the amount of water was selected in such a way as to ensure an even consistency (mini-cone flow diameter) of SSCs (Table 9).

Table 9. Physical and mechanical characteristics of SSC_K with equal consistency at the age of 90 days.

Binder ID	W/S Ratio	Average Density, kg/m^3	Compressive Strength, MPa
SSC_K^{600}	0.37	1795	26.67
SSC_K^{800}	0.35	1844	35.72
SSC_K^{1000}	0.34	1833	30.04

Based on the data, it is clear that with the same consistency of fresh paste, the strength of SSC_K^{800} is 25.3% higher for SSC_K^{600}. Since the difference between the value of mini-cone flow diameter for SSC_K^{600} and SSC_B^{800} with the same value of W/S ratio is significantly greater (Figure 6). There is reason to assume that the decrease in strength of SSC_B^{600} in relation to SSC_B^{800}, while providing the same consistency of SSC, will be even greater than for SSC_K^{600}.

It should be noted that despite the reduction in water content, which is necessary to ensure the same consistency of fresh cement paste, the strength of SSC_K^{1000} is 16% lower than for SSC_K^{800}. Based on the energy consumption for calcination and grinding processes, as well as taking into account physical and mechanical characteristics, it can be assumed that the use of FAB produced at 1000 °C will be the least effective for the production of SSC.

Thus, FAB, as a sulfate component obtained at the calcination temperature of FG at 800 °C, is the most rational from the point of view of energy consumption and physical and mechanical properties of SSCs. For the production of SSC-based products, which are not sensitive to the water consumption of components (for example, production by the method of pressing), the use of SSC^{600} is also possible. This will provide an additional reduction in energy consumption when FAB production.

Based on the obtained experimental data, it is possible to formulate the following assumptions about the implementation of structure formation in SSC:

1. When production of SSC_K with the maximum content of PC (7% of GBFS) and FAB (25% of GBFS), which is characterized by high pH values (11.9–12.5), the most favorable conditions for alkaline activation of slag are provided, with the release of a large number of Si^{4+} and Al^{3+} ions, which actively interact with the extra amount of SO_4^{2-}. This leads to the formation of ettringite and gel CS(A)H, which up to 7 days, contributes to the most intense increase in strength. In the future, most likely due to the formation of an excessively compact layer of new formations on the surface of the slag and blocking ion exchange with the porous medium, the reaction begins to slow down. The intensity of hardening of the SSC due to the content of PC after 7 days of hardening is also significantly reduced due to the consumption of the main part of the clinker substance and the blocking of its residues. The ability of FAB to self-harden is relatively low in the entire studied time interval, so it cannot provide a noticeable strengthening of the SSC.
2. A lower content of FAB_K in the SSC promotes smoother hydration processes. Probably, this is due to a decrease in the degree of alkaline activation of slag. This is weakly reflected in the early strength, which is mainly provided by PC. However, in the later period of hardening, the strength of SSC_K containing 15% of FAB exceeds the strength of SSC_K with 25% of FAB. Also, this phenomenon is facilitated by the increase in the content of GBFS in the SSC, as the main source of Si^{4+} and Al^{3+} ions, which are responsible for SSC hardening.
3. The above-mentioned makes it possible to assume that the key factor affecting the rate and efficiency of SSC hardening is the provision of a rational degree of activation of GBFS, when the ion exchange between the surface of the solid phase and the liquid phase in the pore space of the binder is sufficiently intense and long-lasting. This is greatly facilitated by the increase in the area of the active surface of GBFS due to the increase in dispersion (this factor is not considered in the framework of this study) or its content in the SSC, which increases with a decrease in the content of FAB and PC.
4. An increase in the pH value and (or) content of FAB contributes to an increase in the initial rate of hardening, but also increases the coefficient of inhibition of this process. Accordingly, for different types of FAB, depending on their genetic characteristics, the rational degree of activation of GBFS will be reached at different contents of FG

depending on its pH value.

In the case of SSC_B with the maximum content of PC, the tendency to decrease strength with increasing content of FAB_B is observed at earlier periods of hardening, which is probably associated with lower pH values of FAB_B, as one of the significant factors of intensification of GBFS hardening. This, together with a decrease in the emission of ions associated with a decrease in the reactive surface of GBFS in SSC, negatively affects the volume of new formations and the hydration process.

5. A decrease in PC content in the SSC_B from 7% to ≈3.5%, which provides its own contribution to the hardening of the SSC and is an alkaline activator, initiates a decrease in strength, regardless of the content of FAB in the binder. Most likely, in this case, the PC content is still insufficient for the effective alkaline activation of the slag. At the same time, new formations of PC paste settle on the surface of the slag, which is the most represented crystallization substrate, and block access to it. The increase in FAB content is not significant, but it also negatively affects the compressive strength. This can be explained by the prevalence of reduction in the active surface of slag over the activating effect of FAB. At the same time, the tendency to decrease is most pronounced when using FABB, which is explained by its lower pH value and smaller contribution to the GBFS activation process.
6. Further reduction in PC content from 3.5% to 0%, FAB turns out to be the main agent that activates the hydration of GBFS. At the same time, when the presence of FAB_B (with a lower pH value), the structure formation and hardening of the SSC_B proceeds mainly through the mechanism of sulfate activation. The dissolution of slag under the action of ions proceeds much more slowly than in a medium with a high pH value. This causes a slower and smoother set of strength with a low braking coefficient of this process, but also lower ultimate strength in the considered time interval.

   In the case of using FAB_K (with a high pH value), probably, the alkaline mechanism of activation remains predominant. The absence of PC has a negative effect on the early strength, but at the same time, one of the factors blocking the slag surface is excluded, and its relative amount in the system increases, which reduces the degree of inhibition of the hardening system and provides the highest strength in the late hardening period (90 days).

3.2.5. Effect of Composition and Technological Parameters on pH Value in the Pore Space of SSC Samples at the Age of 28 Days

After processing the experimental data, regression equations were obtained that allow describing the effect of variable factors on the pH value in the pore space of SSC at the age of 28 days (Equations (21) and (22)).

$$pH_K{}^{28} = 10.98 + 0.01X_1 + 0.19X_2 + 0.04X_3 + 0.09X_1^2 + 0.11X_2^2 - 0.03X_1X_2 - 0.03X_1X_3 - 0.01X_2X_3 \quad (21)$$

$$pH_B{}^{28.} = 11.16 - 0.03X_1 + 0.57X_2 - 0.08X_3 - 0.04X_1^2 - 0.43X_2^2 - 0.13X_3^2 + 0.01X_1X_3 + 0.11X_2X_3 \quad (22)$$

Analysis of regression Equations (21) and (22) showed that PC content in the mixture (factor X_2) is the most significant of the three variable factors affecting the growth of pH_{28} values, regardless of the type of FAB. The importance of this factor increases in the solidified SSC, as evidenced by the large values of coefficients for X_2 in Equations (21) and (22) compared to similar coefficients in Equations (3) and (4). Also, the general character of the influence of FAB content (factor X_1) and calcination temperature of FG (factor X_3) on pH value is preserved.

When comparing the regression Equations (21) and (22), it was also established that the pH values in the solidified SSC at "zero" values of the variable factors compared to the initial level were reduced. For SSC_B, the pH value decreased to 11.16 (Equation (22))

relative to the initial value (pH = 11.49, Equation (4)), and for SSC_K, the pH value decreased to 10.99 (Equation (21)) relatively to the initial value (pH = 11.76, Equation (3)).

The profile of the nomogram describing the dependence of pH_{28} on various factors has practically not changed (Figure 10), and is similar to the profile of the pH value nomogram for SSC in an aqueous extract (Figure 4). A decrease in pH values at the age of 28 days compared to the initial pH value is most likely connected with the process of carbonization in the system and binding of part of calcium hydroxide in new formations. According to the data presented in [14], carbonization of ettringite occurs at the first stage with the formation of $CaCO_3$ and $CaSO_4$ (Equation (23)). CSH and CAH gels are carbonized much more slowly at a later hardening period, transforming into a gel with a high degree of polymerization and a low CaO/SiO_2 ratio (Equation (24)), which contributes to the formation of capillary pores. Together, these processes can lead to a loss in strength.

$$3CaO{\cdot}Al_2O_3{\cdot}3CaSO_4{\cdot}32H_2O + 3H_2CO_3 \rightarrow 3CaCO_3 + 3CaSO_4 + Al_2O_3{\cdot}XH_2O + (35 - X)\,H_2O \quad (23)$$

$$XCaOx{\cdot}YSiO_2{\cdot}H_2O + XH_2CO_3 \rightarrow XCaCO_3 + YSiO_2 + (X + 1){\cdot}H_2O \quad (24)$$

However, the absence of a decrease in compressive strength at the age of 90 days (Figure 9) gives reason to assume the following: (1) $CaCO_3$, formed in the SSC, acts as a capillary pore filler and prevents further penetration of carbon dioxide into the SSC; (2) $CaSO_4$, formed during carbonation, can further participate in the hydration reaction, which is consistent with the results and conclusions that were obtained earlier [14].

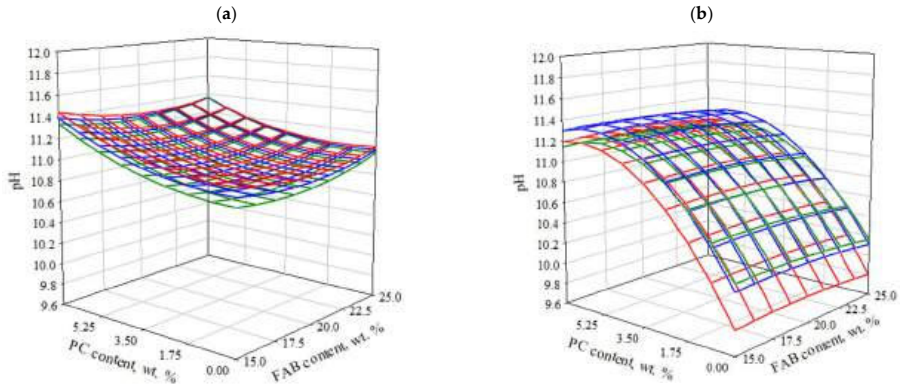

Figure 10. The effect of the content of FAB_K (**a**), FAB_B (**b**), and PC, on the pH value of the aqueous extract of SSCs at different calcination temperatures of FG: ■—600 °C; ■—800 °C; ■—1000 °C.

3.3. Morphology and Type of New Formations

The analysis of new formations was carried out with scanning electron microscopy and X-ray phase analysis of SSC samples at the age of 28 and 90 days. Mixes 11, 15, and 12, containing 20% of FAB^{800} and, respectively, 7%, 3.5%, and 0% of PC, were used as research objects (Table 6).

3.3.1. Morphology of New Formations

Analysis of the microstructure of solidified SSCs at the age of 28 and 90 days showed that the content of PC and the type of FAB affect the amount of morphology of new formations. In particular, SSC with the maximum PC content (7%, Mix 11, Table 6) is characterized by a compact structure with a large proportion of hydration products, regardless of the type of FAB (Figure 11). At the same time, in SSC_K (Figure 11a) compared to SSC_B (Figure 11b), a larger amount of needle and columnar crystals of ettringite (AFt) are observed, which form joints in the pore space and intertwine with the flaky and fibrous CSH-phase, forming a rather compact system of new formations. The structure of SSC_B is mostly represented by foil-like and fibrous CSH, columnar crystals of ettringite, and their joints are also visible in

the pore space (Figure 11b). At 90 days, in both cases, regular compaction of the structure is observed (Figure 11). At the same time, sufficiently large areas of CSH are identified in SSC_K.

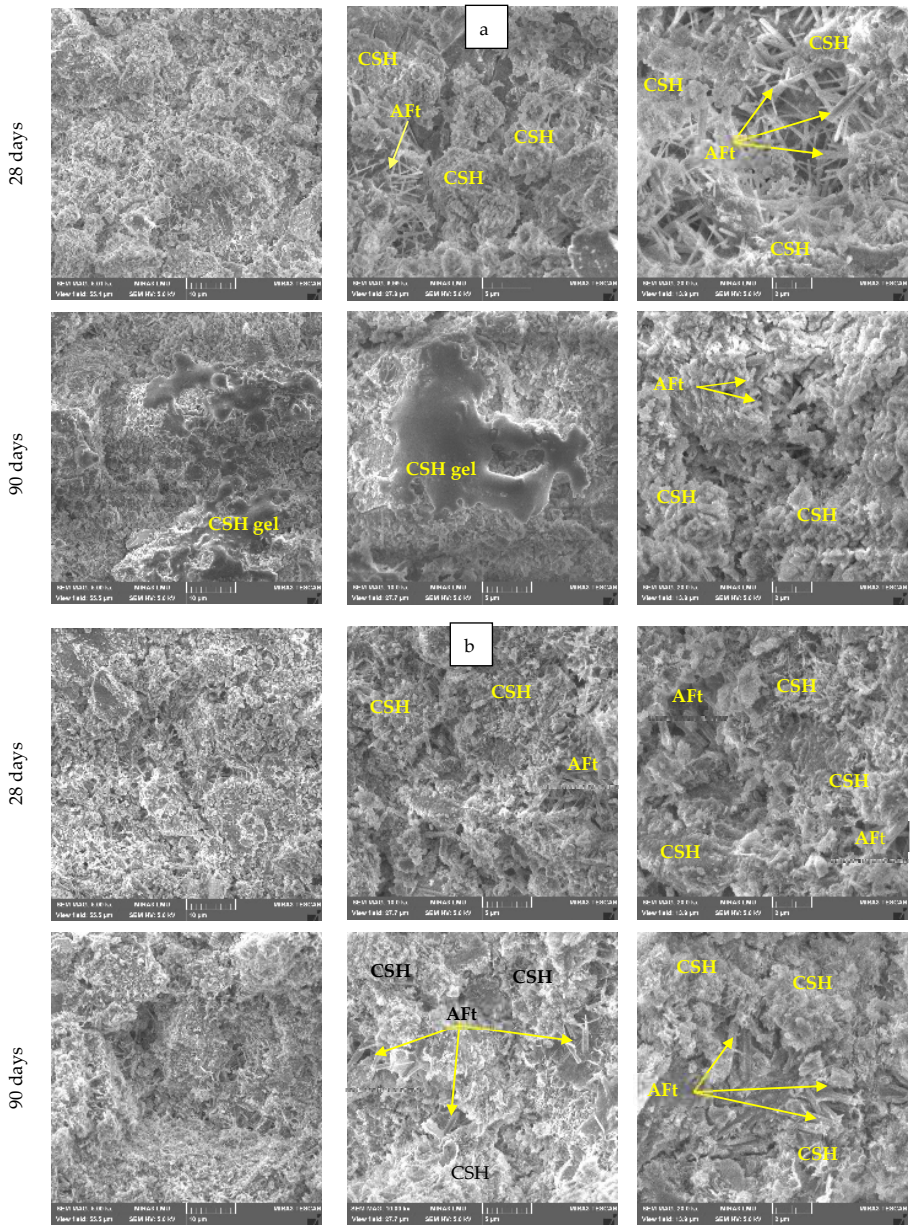

Figure 11. Morphology of new formations in SSC_K (**a**) and SSC_B (**b**) (Mix 11, Tables 7 and 8).

Thus, at the maximum content of PC in SSC_K and SSC_B, insignificant differences in the morphology of new formations are observed, which, most likely, are predetermined by the difference in pH values for binders both at the initial stage and during the hardening process.

Reducing the content of PC from 7% to 3.5% (Mix 15, Table 6) helps reduce the number of new formations. Large grains of GBFS are visible in the system, while the proportion of needle-like newly formed ettringite, which intersects with the fibrous CSH-phase, increases (Figure 12). In this case, the surface of the hydration product is looser, which predetermines the lower compressive strength of SSC with 3.5% of PC compared to SSC with 7% of PC. At 90 days, an increase in the average density of the SSC and the content of columnar crystals of ettringite is observed in both SSCs (Figure 12), which is the main factor in the strength growth of these in the period from 28 to 90 days.

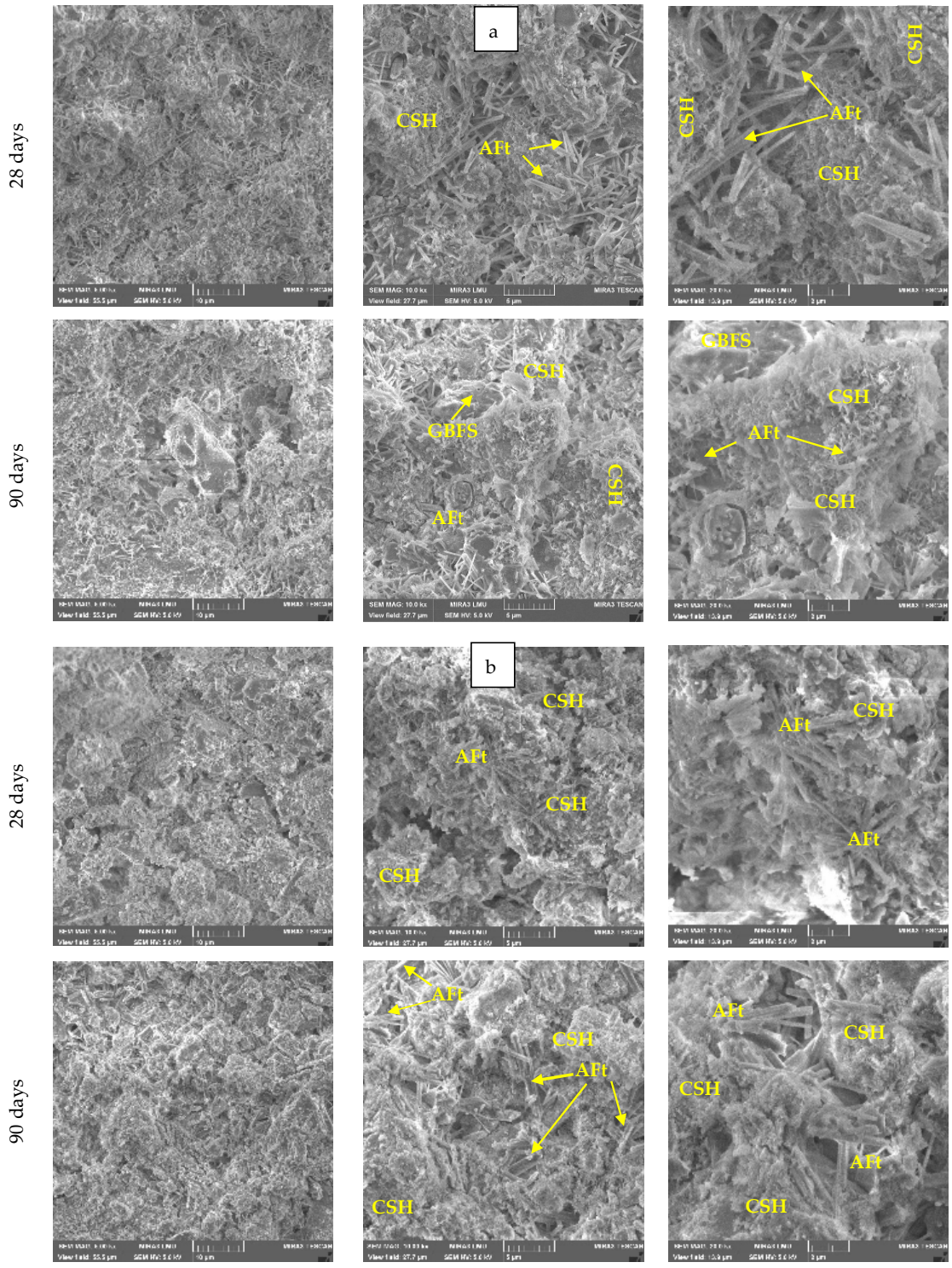

Figure 12. Morphology of new formations in SSC_K (**a**) and SSC_B (**b**) (Mix 15, Tables 7 and 8).

Thus, reducing the content of PC in SSC from 7% to 3.5% slows down the process of structure formation and contributes to the formation of a less compact and less strong crystal structure.

After the compressive strength test for free-of-cement SSC_K, it was found that the inner part of the samples hardened for 90 days is darker than the others and has a greenish color (Figure 13b). At the same time, an insignificant area of the sample around the perimeter has a standard color. A clear border between the two areas was visible both under a microscope and without magnification.

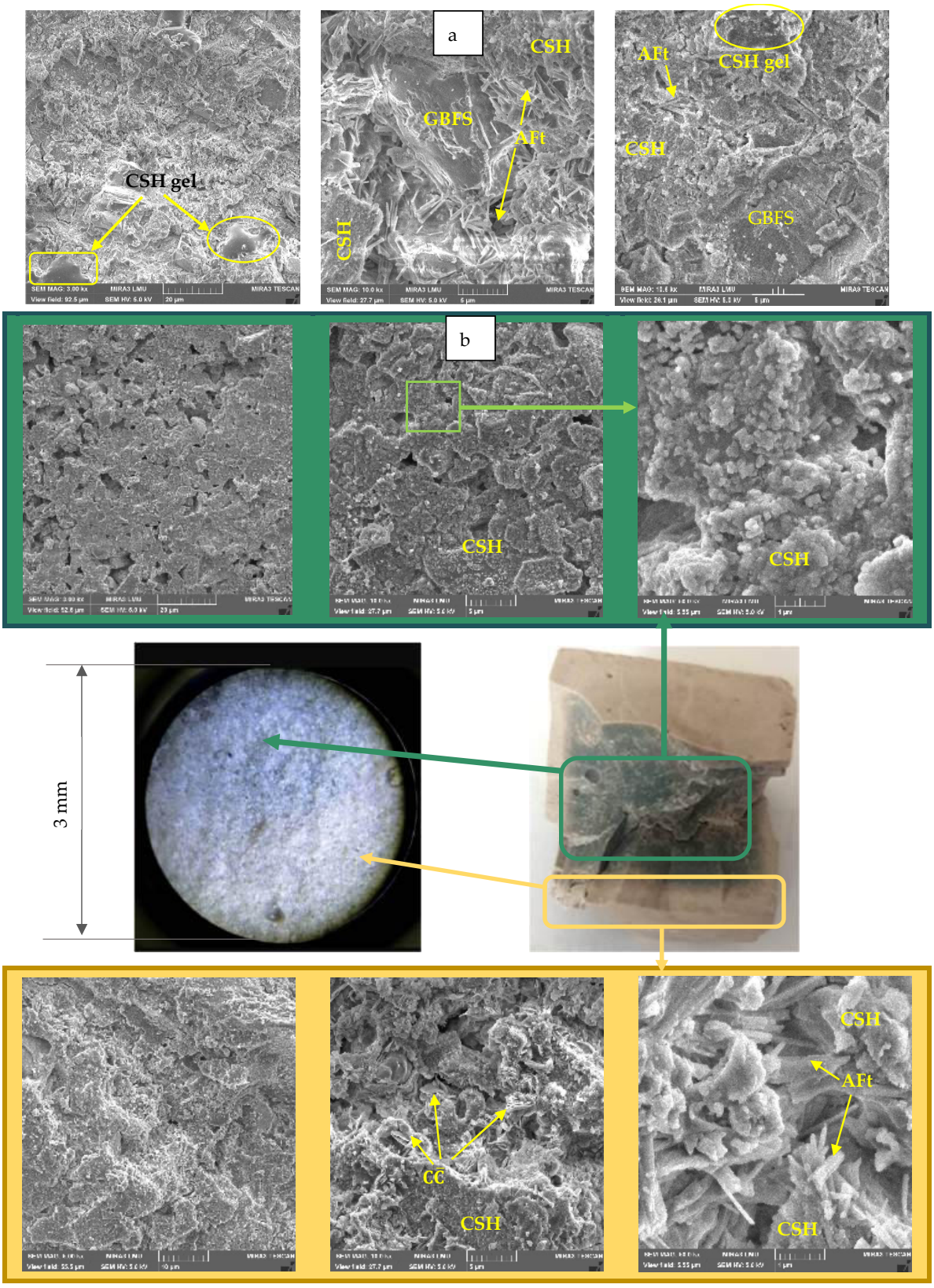

Figure 13. Morphology of new formations in SSC_K (Mix 12, Table 7) (**a**) at 28 days (**b**) at 90 days.

The study of the microstructure of free-of-cement SSC_K made it possible to establish that at the age of 28 days, compared to Mixes containing PC (Figures 11a and 12a), they naturally differ in a significantly smaller number of ettringite crystals and CSH-phase, and a large amount of GBFS grains is also visible (Figure 13a). It should be noted that, as in the

case of SSC_K with 7% of PC (Figure 13a) studied at the age of 90 days, in the free-of-cement SSC_K at the age of 28 days, areas of CSH are identified, although in smaller quantities.

The "green" and "light" areas of SSC_K samples at the age of 90 days were studied by SEM microscopy. As a result of the research, a significant difference in the morphology and density of new formations was revealed.

"Light "area, represented mainly by fibrous CSH-phase and intergrowths of lamellar crystals of calcium carbonate ($C\overline{C}$). Short crystals of ettringite were identified in small quantities at high magnification (Figure 13b). The presence of calcium carbonate demonstrates that the "light zone" is the zone of carbonization.

"Green zone" is characterized by greater density, while separate structural units such as ettringite and calcite are not identified in it. Most likely, it mostly consists of encapsulated CSH-phase.

In a number of studies [26–28] it was shown that concrete produced using GBFS and PC under certain conditions has the property to acquire a blue-green color. This coloration, sometimes referred to as a "greening effect". According to a number of studies [26–28], the reason for the "greening effect" may be the presence of iron in the slag. In particular, in the work [26], the authors note that at high temperatures when the GBFS production, iron compounds and sulfides react, forming iron sulfides, which are partially oxidized under the action of oxygen and change color from black to brown, and partially remain in the highly developed pore space of GBFS. When using GBFS as a component of the concrete mixture, iron sulfides present in GBFS decompose during hydration with the formation of limonite (hydrated iron oxide) and iron sulfate crystallite (hydrated iron sulfate). Iron sulfate hydrate is found in two forms: (1) siderotilate ($FeSO_4$ $5H_2O$), which has a "greenish" color; (2) rosenite ($FeSO_4$ $7H_2O$) has a blue-green color. These two compounds are responsible for the color of wet GBFS-based concrete. As oxygen enters the depth of the hardening matrix and the loss of crystallization water as a result of drying, iron salts are oxidized to trivalent salts, which leads to a change in color from blue-green to brown. In the study [26], the following relationship was established: the higher the density and strength of concrete consisting of GBFS (50%) and PC (50%), the greater the blue-green area in the sample volume. That is, the "greening effect" can act as an indicator of the density and, as a result, the strength of concrete.

Thus, based on the fact that free-of-cement SSC_K samples have a greenish-blue color in the main volume and characterized by a high compressive strength (50 MPa), it is possible to make an assumption that the absence of PC in the SSC significantly slowed down the activation of slag and the decomposition of iron sulfide into iron sulfates. This is evidenced by the slow growth of the strength of these binders, as well as the absence of a greenish color in the samples up to 28 days. During the further hardening of free-of-cement SSC_K, such conditions were created that led to the formation of iron sulfates and compactly arranged new formations, which provides preservation of the "greening effect" inside the samples.

Analysis of the morphology of new formations in free-of-cement SSC_B showed that at the age of 28 days, SSC_B is mainly represented by fibrous CSH-phase, covering the surface of GBFS grains with a thin layer (Figure 14). At the same time, there are no ettringite crystals, so the SSC_B has the lowest compressive strength. At 90 days, the compaction of the SSC_B and the coating of the slag surface with new formations are observed.

In this case, the change in the color of the samples was not observed, which is probably related to the lower pH value of FAB_B. As a result, the activation process in GBFS is much slower than in SSC_K. However, it is not excluded that the color of the samples will change at later stages of hardening.

Thus, based on the obtained results, it is possible to conclude that the slower activation of slag when the absence of PC in the SSC significantly slows down the process of structure

formation and strength growth of free-of-cement SSC. However, pH values contribute to the formation of a more homogeneous system of new formations and a less permeable matrix, with high compressive strength at later stages of hardening.

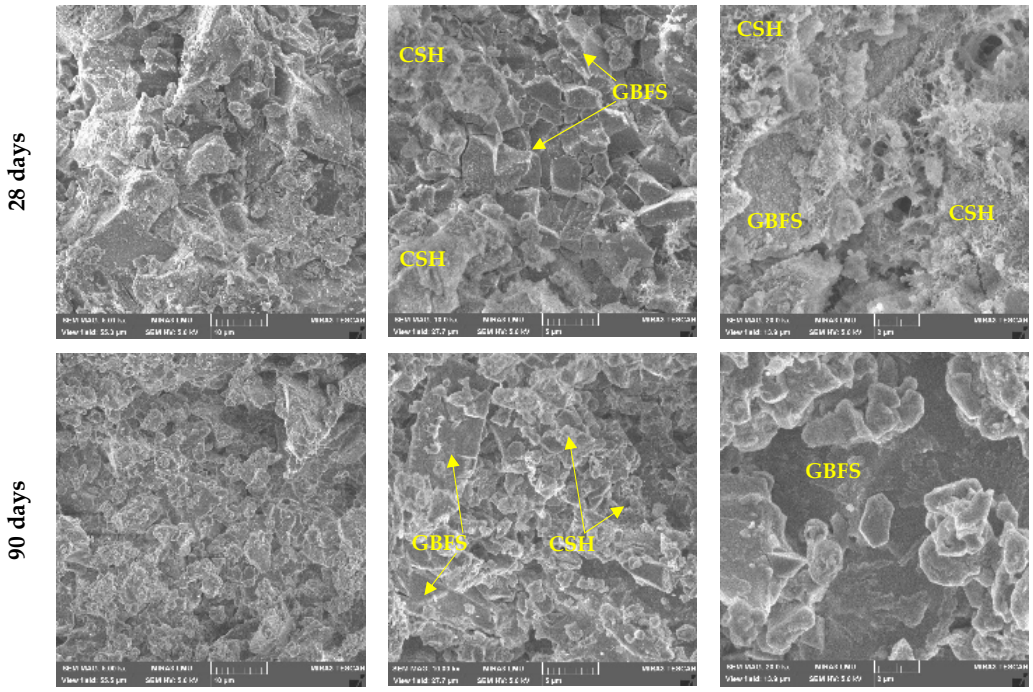

Figure 14. Morphology of new formations in SSC_B (Mix 12, Table 8).

3.3.2. XRD Analysis of New Formations

It is necessary to note that the identification of new formations in SSC with XRD analysis is very difficult, especially when identifying calcium hydrosilicates and hydroaluminates. This is due to the fact that $CaSO_4$, obtained from FG, used as a sulfate component, has a distinct main peak, and some of the peaks intersect or overlap with ettringite peaks. In this regard, when recognizing XRD profiles of SSC, the main attention was directed to establishing regularities of changes in the intensity of the peaks of phosphoanhydrite, ettringite, and calcite.

The comparison of SSC_K X-ray profiles showed that the samples (Figure 15) at the age of 90 days compared to the 28-day samples have a decrease in the intensity of the main peak of $CaSO_4$, which may indicate that the processes of structure formation with the participation of FAB continue even at later periods of hardening (after 28 days). Also, in these SSCs, pronounced ettringite peaks are observed regardless of the composition and duration of hardening. In these binders, the peak of calcite is also identified at the age of 28 days, while its intensity in SSC_K with 7% PC content practically does not change over time (Figure 15a). This may indicate the decay of carbonation processes. Also, when the content of the alkaline component decreases, the intensity of the $CaCO_3$ peak increases. At the age of 90 days, the maximum growth intensity of the $CaCO_3$ peak is observed for free-of-cement SSC_K (Figure 15c).

More intense carbonization in SSC_K with 3.5% PC content (Mix 15, Table 7) and in free-of-cement SSC_K (Mix 12, Table 7) is explained by the fact that in the initial period of hardening, they differ in lower average density (Table 6), and therefore greater permeability for CO_2.

The comparison of XRD profiles for SSC_B showed that in the samples with the maximum content of PC (Figure 16a) and in the free-of-cement samples (Figure 16b) at the age of 90 days compared to the 28-day-aged samples, there is practically no change in the

intensity of the main peak of $CaSO_4$, which may indicate that FAB in these mixes does not participate in the structure formation at a later hardening period. Strength growth in this case occurs either due to the further formation of calcium hydrosilicates during GBFS hydration, or due to the recrystallization of previously formed new formations. It is also necessary to note that these binders differ in more pronounced ettringite peaks compared to free-of-cement SSC_B (Figure 15b). This is in agreement with data on the morphology of new formations in SSC_B, during which the absence of ettringite in free-of-cement SSC_B was established (Figure 14).

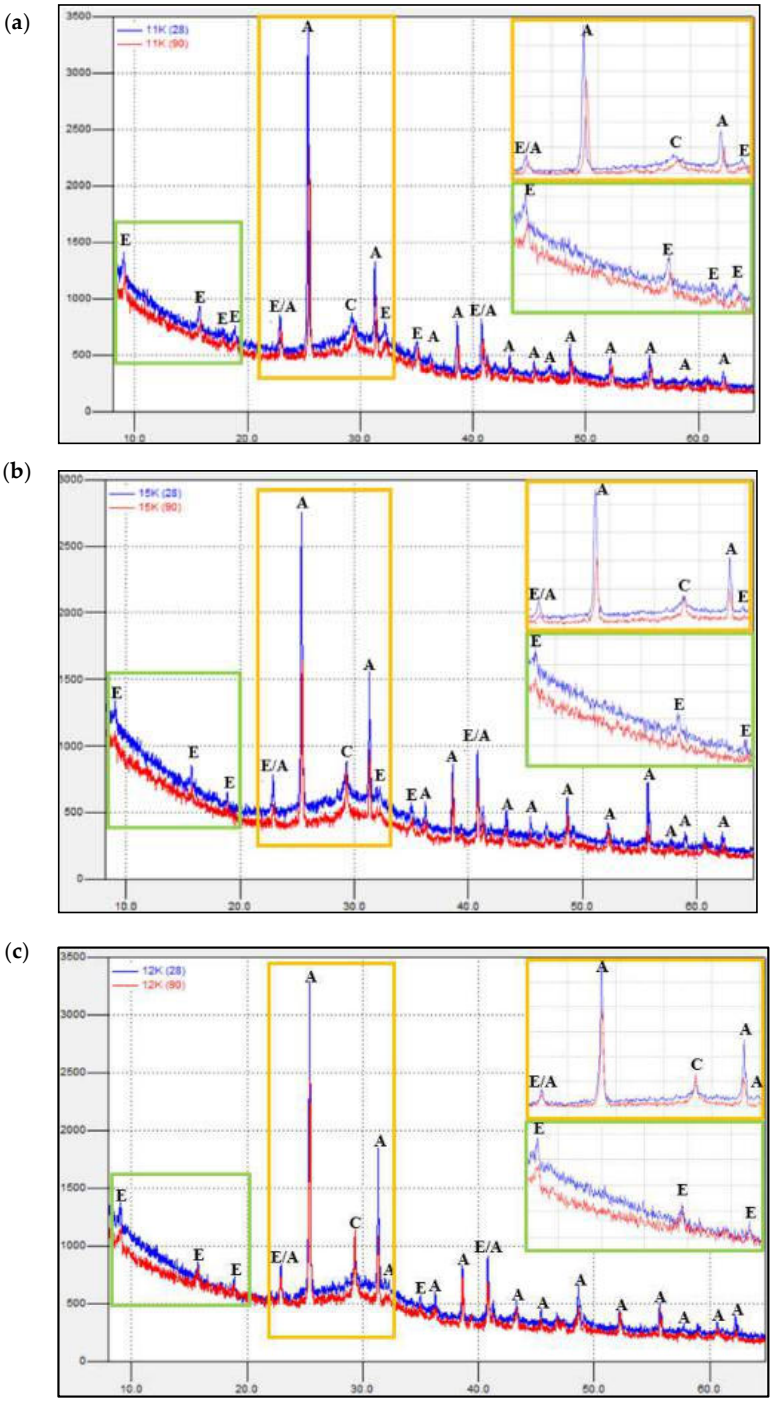

Figure 15. XRD profiles for SSB_K with different composition: (**a**) Mix 11; (**b**) Mix 15; (**c**) Mix 12 (Table 7) E—ettringite; A—anhydrite; C—calcite.

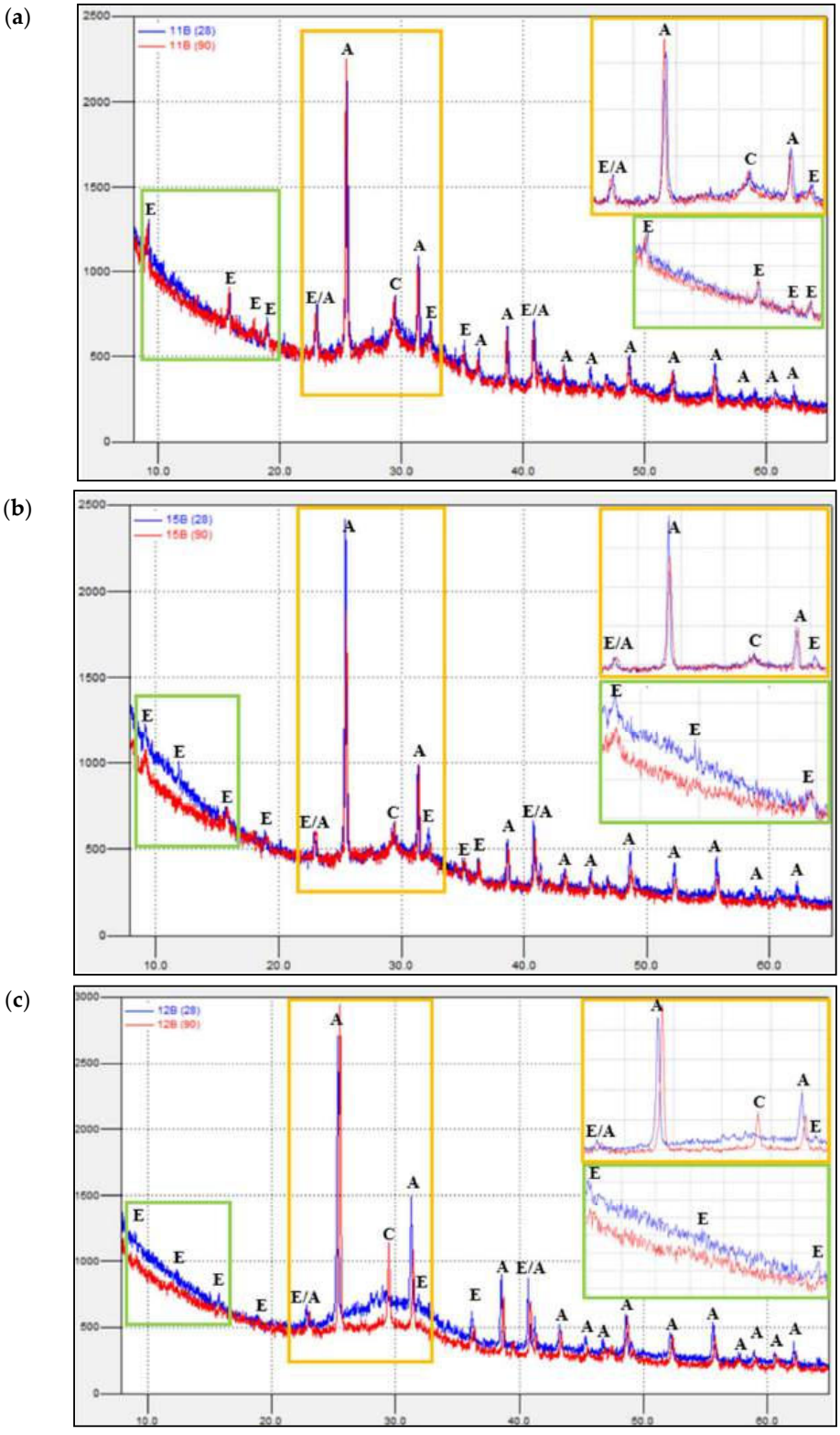

Figure 16. XRD profiles of SSC_B with different compositions: (**a**) Mix 11; (**b**) Mix 15; (**c**) Mix 12 (according to Table 8) E—ettringite; A—anhydrite; C—calcite.

It should also be noted that for SSC_B containing PC (Figure 16a,b), the calcite peak appears already at the age of 28 days, and the intensity of the calcite peak practically does not change by 90 days, which indicates the slowing down of carbonation.

For free-of-cement SSC_B, at the age of 28 days, the calcite peak is practically not observed, but it becomes more pronounced at 90 days. This is due to the fact that carbonation

in SSC, first of all, goes to ettringite, the amount of which is extremely low. Further, after 28 days, carbonation most likely occurs through calcium hydrosilicates (Equation (24)), which causes the appearance of a calcite peak.

4. Conclusions

Based on the research, the following conclusions are formulated:

Differences between the studied FGs and calcination temperature cause differences between FABs obtained on their basis. The most important factors that depend on the type of FG and calcination temperature and have an effect on the properties of SSC are particle morphology and pH value.

It is established that the morphology of FAB particles obtained at 600 °C, regardless of FG type, is similar to the morphology of initial FG particles. An increase in the calcination temperature to 800 °C and 1000 °C contributes to the melting of particles, compaction of their surface, and, as a result, a decrease in porosity and specific surface area. A positive effect of surface compaction of FAB particles is a decrease in water consumption of SSC, which is favorably reflected in the physical and mechanical characteristics of SSC. The negative effect is an increase in the density and hardness of particles, which leads to an increase in the energy consumption of the grinding process. In addition, the reactivity of FAB decreases, which negatively affects the strength of SSC.

Among the calcination temperatures that were used for the production of FAB, 800 °C is the most favorable in terms of the balance between positive and negative effects on SSC properties. However, FAB_B probably has a certain reserve for lowering the calcination temperature, which is evidenced by the absence of particles with morphology similar to the original FG_B in FAB_B^{800}, and sufficiently high mini-cone flow diameters for SSC_B^{800}, comparable to the indicators for SSC_B^{1000}. Lowering the calcination temperature will allow for a reduction in the cost of calcination and grinding, and, probably, may have a positive effect on the reactivity of FAB and the strength of SSC_B.

The presence of particles with morphologies similar to the original FG (loose and highly developed surface) in the FAB_K^{800} raises the question of considering the possibility of increasing the duration of calcination of FG_K at 800 °C or increasing the calcination temperature to ensure compaction and rearrangement of particles. However, it is necessary to keep a balance between physical and mechanical characteristics and energy costs of calcination and grinding.

It is established that the pH value for FG_K and, accordingly, for FAB_K, as well as the calcination temperature, have a significant effect on the structure formation and physical and mechanical properties of SSC_K. At the same time, high pH values for FGB_K not only provide a faster growth in compressive strength over time and its larger values, but they also make it possible to obtain free-of-cement SSC_K with high physical and mechanical characteristics (compressive strength ≈50 MPa) at the age of 90 days. The absence of a bend in the nomograms in the direction of a decrease in strength when the FAB_K content increases from 15 to 25% in free-of-cement SSC_K makes it reasonable to consider the possibility of increasing the FAB_K content above 25%, which significantly increases the volume of FG_K utilization and, together with the exclusion of PC from SSC, increases the eco-friendly effect of its use.

Since there is no unified opinion regarding the “greening effect” and a clear understanding of the reasons for its occurrence in the literature. Therefore, it appears that it is extremely important to further identify factors that allow for purposefully ensuring this effect during the production of free-of-cement SSC_K and concrete based on it. This will allow for raising similar materials to a new level of energy efficiency, low carbon, and environmental friendliness.

Author Contributions: Conceptualization, N.A. (Nataliya Alfimova), K.L., I.N. and M.E.; methodology, N.A.(Nataliya Alfimova), K.L., I.N. and M.E.; validation, N.A. (Nataliya Alfimova), K.L., I.N., M.E., N.K. and N.A. (Nikita Anosov); formal analysis, N.A. (Nataliya Alfimova), K.L., I.N., M.E., N.K. and N.A. (Nikita Anosov); investigation, N.A. (Nataliya Alfimova), K.L., I.N., M.E., N.K. and N.A. (Nikita Anosov); resources, N.A. (Nataliya Alfimova), K.L., I.N., M.E., N.K. and N.A. (Nikita Anosov); data curation, N.A.(Nataliya Alfimova), K.L., I.N., M.E., N.K. and N.A. (Nikita Anosov); writing—original draft preparation, N.A.(Nataliya Alfimova), K.L., I.N., M.E., N.K. and N.A. (Nikita Anosov); writing—review and editing, N.A. (Nataliya Alfimova), K.L., I.N., M.E., N.K. and N.A. (Nikita Anosov); visualization, N.A. (Nikita Anosov), K.L., I.N. and M.E.; supervision, N.A. (Nataliya Alfimova), K.L., I.N., M.E., N.K. and N.A. (Nikita Anosov); project administration, N.A. (Nataliya Alfimova), K.L. and I.N.; funding acquisition, N.A.(Nataliya Alfimova), K.L., I.N. and N.K. All authors have read and agreed to the published version of the manuscript.

Funding: The work was realized under support of the State Assignment for the creation of new laboratories in 2021, including under the guidance of young promising researchers of the national project "Science and Universities". The research title is "Elaboration and development of scientific and technological foundations for creating an integrated technology for processing gypsum-containing waste from various industrial enterprises and searching of new ways to use processed products", FZWG-2024-0001. Using equipment of High Technology Center at BSTU named after V. G. Shukhov.

Data Availability Statement: Data are contained within the article.

Acknowledgments: The work was realized under administrative support of the world-class scientific and educational center "Innovative Solutions in the Agricultural Sector" (Belgorod) and under the support of PhosAgro/UNESCO/IUPAC for the project "Development of a method for complex processing of phosphogypsum waste".

Conflicts of Interest: The authors declare no conflicts of interest.

References

1. Luo, W.; Li, B.; Xu, M.; Pang, C.; Lester, E.; Xu, L.; Kow, K.-W. In-situ release and sequestration of CO_2 in cement composites using LTA zeolites. *Sci. Total Environ.* **2023**, *872*, 162133. [CrossRef] [PubMed]
2. Supriya; Chaudhury, R.; Sharma, U.; Thapliyal, P.C.; Singh, L.P. Low-CO_2 emission strategies to achieve net zero target in cement sector. *J. Clean. Prod.* **2023**, *417*, 137466. [CrossRef]
3. Kaliyavaradhan, S.K.; Ling, T.-C. Potential of CO_2 sequestration through construction and demolition (C&D) waste—An overview. *J. CO_2 Util.* **2017**, *20*, 234–242. [CrossRef]
4. Juenger, M.C.G.; Winnefeld, F.; Provis, J.L.; Ideker, J.H. Advances in alternative cementitious binders. *Cem. Concr. Res.* **2011**, *41*, 1232–1243. [CrossRef]
5. Ouyang, G.; Li, Z.; Sun, T.; Ye, Z.; Deng, Y.; Li, W. Greener phosphogypsum-based all-solid-waste cementitious binder with steel slag activation: Hydration, mechanical properties and durability. *J. Clean. Prod.* **2024**, *443*, 140996. [CrossRef]
6. Wu, Q.; Xue, Q.; Yu, Z. Research status of super sulfate cement. *J. Clean. Prod.* **2021**, *294*, 126228. [CrossRef]
7. Gruskovnjak, A.; Lothenbach, B.; Winnefeld, F.; Figi, R.; Ko, S.-C.; Adler, M.; Mäder, U. Hydration mechanisms of super sulphated slag cement. *Cem. Concr. Res.* **2008**, *38*, 983–992. [CrossRef]
8. Zokaei, S.; Siad, H.; Lachemi, M.; Mahmoodi, O.; Ozcelikci, E.; Şahmaran, M. Engineered Cementitious Composites with Super-Sulfated Cement: Mechanical, Physical, and Durability Performance. *Materials* **2024**, *17*, 2240. [CrossRef]
9. Kühl, H. Verfahren zur Herstellung von Zement aus Hochofenschlacke. German Patent No. 237,777, 23 December 1908.
10. *EN 15743:2010+A1:2015*; «Supersulfated Cement—Composition, Specifications, and Conformity Criteria». European Committee for Standardization (CEN): Brussels, Belgium, 2010.
11. Alfimova, N.I.; Levickaya, K.M.; Elistratkin, M.Y.; Bukhtiyarov, I.Y. Supersulfated cements: A review analysis of the features of properties, raw materials, production and application prospects. *Bull. BSTU Named After V.G. Shukhov* **2024**, *7*, 8–24. [CrossRef]
12. Shi, X.; Zeng, A.; Duan, H.; Zhang, H.; Yang, J. Status and development trends of phosphogypsum utilization in China. *Circ. Econ.* **2024**, *3*, 100116. [CrossRef]
13. Wu, F. The treatment of phosphogypsum leachate is more urgent than phosphogypsum. *Environ. Res.* **2024**, *262*, 119849. [CrossRef] [PubMed]
14. Wei, Z.; Deng, Z. Research hotspots and trends of comprehensive utilization of phosphogypsum: Bibliometric analysis. *J. Environ. Radioact.* **2022**, *242*, 106778. [CrossRef] [PubMed]

15. Liu, S.; Ouyang, J.; Ren, J. Mechanism of calcination modification of phosphogypsum and its effect on the hydration properties of phosphogypsum-based supersulfated cement. *Constr. Build. Mater.* **2020**, *243*, 118226. [CrossRef]
16. Xie, Y.; Sun, T.; Shui, Z.; Ding, C.; Li, W. The impact of carbonation at different CO_2 concentrations on the microstructure of phosphogypsum-based supersulfated cement paste. *Constr. Build. Mater.* **2022**, *340*, 127823. [CrossRef]
17. Wang, L.; Gao, Z.; Gao, F.; Li, X.; Chang, S.; Liu, S. Comparing study on the evolution characteristics of performance and microstructure between Portland slag cement and supersulfated cement under chemical attacks. *Constr. Build. Mater.* **2024**, *425*, 135969. [CrossRef]
18. Pinto, S.R.; da Luz, C.A.; Munhoz, G.S.; Medeiros-Junior, R.A. Durability of phosphogypsum-based supersulfated cement mortar against external attack by sodium and magnesium sulfate. *Cement. Concr. Res.* **2020**, *136*, 106172. [CrossRef]
19. Liu, S.; Wang, L.; Yu, B. Effect of modified phosphogypsum on the hydration properties of the phosphogypsum-based supersulfated cement. *Constr. Build. Mater.* **2019**, *214*, 9–16. [CrossRef]
20. Bilal, E.; Bellefqih, H.; Bourgier, V.; Mazouz, H.; Dumitraş, D.-G.; Bard, F.; Laborde, M.; Caspar, J.P.; Guilhot, B.; Iatan, E.-L.; et al. Phosphogypsum circular economy considerations: A critical review from more than 65 storage sites worldwide. *J. Clean. Prod.* **2023**, *414*, 137561. [CrossRef]
21. Levickaya, K.; Alfimova, N.; Nikulin, I.; Kozhukhova, N.; Buryanov, A. The Use of Phosphogypsum as a Source of Raw Materials for Gypsum-Based Materials. *Resources* **2024**, *13*, 69. [CrossRef]
22. Gordashevsky, P.F.; Dolgorev, A.V. *Production of Gypsum Binders from Gypsum-Containing Waste*; Stroyizdat: Moscow, Russia, 1987; 105p.
23. Akhmedov, M.A.; Atakuziev, T.A. Phosphogypsum. In *Research and Application*; Fan: Tashkent, Uzbekistan, 1980; 156p.
24. Schmid, T.; Jungnickel, R.; Dariz, P. Insights into the $CaSO_4$–H_2O System: A Raman-Spectroscopic Study. *Minerals* **2020**, *10*, 115. [CrossRef]
25. Klimenko, V.G.; Pavlenko, V.I.; Gasanov, S.K. The Role of pH Medium in Forming Binding Substauces on Base of Calcium Sulphate. *Middle East J. Sci. Res.* **2013**, *17*, 1169–1175.
26. Sioulas, B.; Sanjayan, J.G. The coloration phenomenon associated with slag blended cements. *Cem. Concr. Res.* **2001**, *31*, 313–320. [CrossRef]
27. Couvidat, J.; Diliberto, C.; Meux, E.; Izoret, L.; Lecomte, A. Greening effect of concrete containing granulated blast-furnace slag composite cement: Is there an environmental impact? *Cem. Concr. Compos.* **2020**, *113*, 103711. [CrossRef]
28. Le Cornec, D.; Wang, Q.; Galoisy, L.; Renaudin, G.; Izoret, L.; Calas, G. Greening effect in slag cement materials. *Cem. Concr. Compos.* **2017**, *84*, 93–98. [CrossRef]